AD-A146 471 A COMPARISON OF EVAPORATION DUCT MODELS FOR IREPS (INTEGRATED REFRACTIVE EFFECTS PREDICTION SYSTEM)(U) NAVAL OCEAN SYSTEMS CENTER SAN DIEGO CA W PATTERSON 1/1

UNCLASSIFIED JUN 84 NOSC/TR-960 F/G 20/14 NL

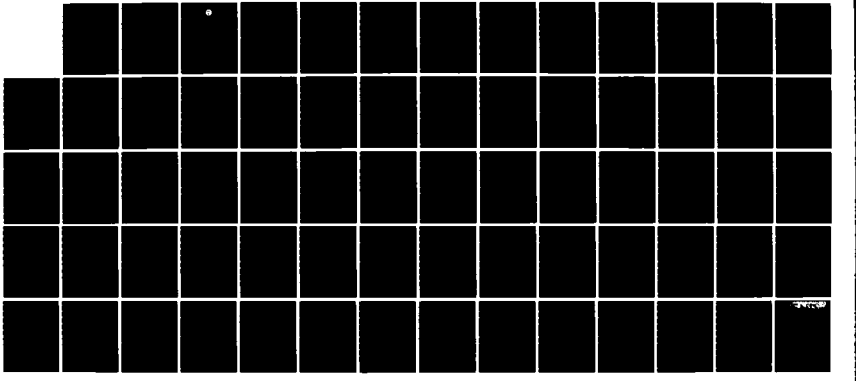

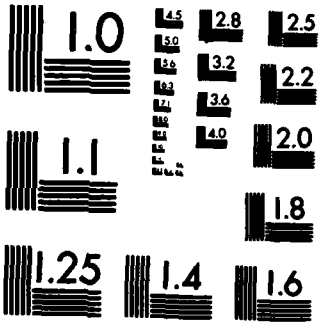

(12)

NOSC TR 960

NOSC TR 960

Technical Report 960

A COMPARISON OF EVAPORATION DUCT MODELS FOR IREPS

W. Patterson

June 1984

Prepared for
Naval Air Systems Command
Code 330

Approved for public release; distribution unlimited

NOSC

NAVAL OCEAN SYSTEMS CENTER
San Diego, California 92152

NAVAL OCEAN SYSTEMS CENTER SAN DIEGO, CA 92152

AN ACTIVITY OF THE NAVAL MATERIAL COMMAND

J.M. PATTON, CAPT, USN
Commander

R.M. HILLYER
Technical Director

ADMINISTRATIVE INFORMATION

The work reported here was sponsored by the Naval Air Systems Command, Code 330, Washington, DC 20362, under program element 62759N.

Released by
J. H. Richter, Head
Ocean and Atmospheric Sciences Division

Under authority of
J. D. Hightower, Head
Environmental Sciences Department

RHB

UNCLASSIFIED

SECURITY CLASSIFICATION OF THIS PAGE

AD-A146 471

REPORT DOCUMENTATION PAGE

1a. REPORT SECURITY CLASSIFICATION UNCLASSIFIED	1b. RESTRICTIVE MARKINGS
2a. SECURITY CLASSIFICATION AUTHORITY	3. DISTRIBUTION/AVAILABILITY OF REPORT Approved for public release; distribution unlimited
2b. DECLASSIFICATION/DOWNGRADING SCHEDULE	
4. PERFORMING ORGANIZATION REPORT NUMBER(S) NOSC TR-960	5. MONITORING ORGANIZATION REPORT NUMBER(S)
6a. NAME OF PERFORMING ORGANIZATION Naval Ocean Systems Center 6b. OFFICE SYMBOL (If applicable)	7a. NAME OF MONITORING ORGANIZATION
6c. ADDRESS (City, State and ZIP Code) Code 5325 San Diego, CA 92152	7b. ADDRESS (City, State and ZIP Code)
8a. NAME OF FUNDING/SPONSORING ORGANIZATION Naval Air Systems Command 8b. OFFICE SYMBOL (If applicable)	9. PROCUREMENT INSTRUMENT IDENTIFICATION NUMBER
8c. ADDRESS (City, State and ZIP Code) Code 330 Washington, DC 20362	10. SOURCE OF FUNDING NUMBERS PROGRAM ELEMENT NO. 62759N; PROJECT NO. SF59551001; TASK NO. SF59551001; WORK UNIT NO. MP33

11. TITLE (Include Security Classification)
A COMPARISON OF EVAPORATION DUCT MODELS FOR IREPS

12. PERSONAL AUTHOR(S)
W. Patterson

13a. TYPE OF REPORT	13b. TIME COVERED	14. DATE OF REPORT (Year, Month, Day)	15. PAGE COUNT
Final	FROM Oct 83 TO Apr 84	June 1984	63

16. SUPPLEMENTARY NOTATION

17. COSATI CODES			18. SUBJECT TERMS (Continue on reverse if necessary and identify by block number)
FIELD	GROUP	SUB-GROUP	Atmospheric Refraction of Electromagnetic Waves Evaporation Ducts IREPS

19. ABSTRACT (Continue on reverse if necessary and identify by block number)

An evaluation of current meteorological measurement techniques to determine adequate description of the surface meteorological processes used to infer evaporation duct height. Includes a comparison of relative performance, sensitivities to meteorological unputs, and ease of computation for several standard evaporation duct height models. EM wave propagation pathloss models are compared and evaluated, and a maximum range of detection error is determined for the modified NOSC propagation model employed by the Integrated Refractive Effects Prediction System (IREPS).

20. DISTRIBUTION/AVAILABILITY OF ABSTRACT	21. ABSTRACT SECURITY CLASSIFICATION	Agency Accession
☒ UNCLASSIFIED/UNLIMITED ☐ SAME AS RPT ☐ DTIC USERS	UNCLASSIFIED	
22a. NAME OF RESPONSIBLE INDIVIDUAL W. Patterson	22b. TELEPHONE (Include Area Code) (619) 225-7247	22c. OFFICE SYMBOL

DD FORM 1473, 84 JAN

83 APR EDITION MAY BE USED UNTIL EXHAUSTED
ALL OTHER EDITIONS ARE OBSOLETE

UNCLASSIFIED

SECURITY CLASSIFICATION OF THIS PAGE

OBJECTIVES

1. Evaluate the current meteorological measurement technique to determine if it is sufficient to adequately describe the surface meteorological processes used to infer evaporation duct height.

2. Compare relative performance, sensitivities to meteorological inputs, and ease of computation for the evaporation duct height models developed by Jeske, Rotheram, and Davidson.

3. Compare and evaluate the EM wave propagation pathloss models developed by Rotheram and the Naval Ocean System Center (NOSC).

4. Determine a maximum range of detection error for the modified NOSC propagation model as employed by the Integrated Refractive Effects Prediction System (IREPS).

RESULTS

1. The evaporation duct height models of Jeske, Rotheram, and Davidson function equally well with reasonable duct heights calculated when considering the statistical average of meteorological inputs.

2. The meteorological observations taken by operational personnel are not of sufficient quality to insure proper duct height calculations when individual duct height predictions are desired.

3. When considering statistical means in observational data, the pathloss models of Rotheram and NOSC performed reasonably well.

4. The assumption of a homogeneous atmosphere for a fleet operational propagation loss model, is reasonable.

5. The theory behind calculation of duct height and pathloss values is statistically sound.

RECOMMENDATIONS

1. Quality of individual meteorological observations needed as input to current state-of-the-art propagation models is insufficient. This can be improved by (a) improving the observational skills of the individual through further training, and (b) developing a sensor system that can be deployed away from the observation platform.

2. Develop an entirely new duct height model using statistical techniques.

3. Design controlled experiments to investigate the role of each assumption upon the actual pathloss over the propagation path.

4. Train fleet operators of the IREPS model in the limitations and recognition of situations in which the model's performance is marginal or poor.

5. Undertake further evaluation of the IREPS model by comparing a predicted range with an actual observed maximum detection range.

CONTENTS

INTRODUCTION

BACKGROUND

The atmosphere is in a constant state of turbulence because of differential solar heating. This turbulence produces a continual variation in horizontal and vertical temperature and moisture gradients.

As electromagnetic (EM) waves propagate through this medium of varying temperature and moisture, they refract, or "bend." A measure of the degree of refraction is the refractive index (n). A time averaged, or "standard," atmosphere will bend a horizontally propagating electromagnetic wave downward with a curvature less than the curvature of the earth's surface. If the refraction is sufficiently great to cause a downward curvature that exceeds the earth's surface curvature, then the propagating electromagnetic wave will be channeled in a "duct." Close to the earth's water surface, less than approximately 30 meters, atmospheric refraction is dominated by evaporation and any duct so formed is called an evaporation duct.

Typically, atmospheric water vapor content over ocean areas will rapidly decrease with height. As a result, at some height, the refractive index gradient will decrease below that value required for ducting. The height of this critical refractive index gradient value is known as the evaporation duct height (δ).

Evaporation ducts are routinely observed over the world's oceans, with increasing frequency and larger duct heights being found at low latitudes, during the summer season, and during daylight hours.

Since the channeling of electromagnetic energy can lead to greatly extended ranges for radar detection of surface targets, and conversely, greater counter-detection ranges, knowledge of n and δ becomes vital for tactical operations. In addition, δ serves as an input parameter to various mathematical models to predict pathloss, and thus, a detection/communication range.

In practice, direct measurement of δ is not possible with a radiosonde or refractometer. The duct height must be inferred from meteorological processes occurring at the air/ocean interface.

PURPOSE

The purpose of the work reported here was to accomplish four objectives.

Objective I

Evaluate the current meteorological measurement technique to determine if it is sufficient to adequately describe the surface meteorological processes used to infer δ.

Objective II

To compare relative performance, sensitivities to meteorological inputs, and ease of computation for the evaporation duct height models developed by Jeske (ref 1), Rotheram (ref 2), and Davidson (ref 3).

Objective III

To compare and evaluate the EM wave propagation pathloss models developed by Rotheram (ref 2) and the Naval Ocean Systems Center (NOSC) (ref 4).

Objective IV

To determine a maximum range of detection error for the modified NOSC propagation model as employed by the Integrated Refractive Effects Prediction System (IREPS).

METHODS

OBJECTIVE I

The theoretical framework for calculation of δ used by all three models under consideration is proposed by Monin and Obukhov (ref 5) and is based upon the relation of surface layer profiles of temperature, moisture, and turbulence with surface fluxes of momentum, sensible heat, and latent heat.

Multilevel measurements needed to determine these surface fluxes are extremely difficult and are operationally beyond the capability of field meteorologists around the world. For this reason, a "bulk" measurement method is sought. If the Monin-Obukhov expressions for temperature, moisture, etc. are expressed as mathematical derivatives, then the integral from a rough surface boundary (z_o) to some reference height (z) will express the fluxes. This introduces two integration boundary conditions. By making certain assumptions about the meteorological conditions at z_o, only the four variables of air temperature (T_a), sea-surface temperature (T_s), moisture (Rh), and wind velocity (U), all measured at z, and the determination of z_o need to be made to determine these fluxes. These meteorological measurements then are referred to as "bulk" measurements.

The models developed by Davidson uses these "bulk" meteorological measurements to explicitly calculate drag coefficients which are used in turn to calculate an atmospheric stability factor. This calculated stability factor is used to define a stability function. From the stability function, the fluxes of temperature, etc. are calculated. Finally, these fluxes are used in an implicit manner to calculate δ.

The models employed by Jeske and Rotheram uses the "bulk" meteorological measurements to calculate a refractive difference between z and z_o, a scale length empirically derived from the Bulk Richard's number, and a profile coefficient. Based upon two empirically derived stability functions, the refractive difference and the scale length are used to explicitly calculate δ.

To achieve the first objective of evaluating the "bulk" meteorological measurements technique, observational meteorological and pathloss data gathered during an extensive experimental program in the eastern Mediterranean (ref 6) are used. During the four months of February, April, August, and November of 1972, radio propagation measurements for frequencies of 1.0426 GHz (L-band), 3.0075 GHz (S-band), 9.624 GHz (X-band), 17.9648 GHz (KU-band), and 37.44 GHz (KA-band) were taken across the Aegean Sea between the islands of Naxos and Mykonos, a horizontal path of 35.2 km. For a transmitter height of approximately 5 meters above mean sea level (MSL) and receiver heights of approximately 5, 10, and 19 meters above MSL, propagation measurements were made at 15-minute intervals.

Meteorological measurements of T_a, T_s, Rh, and U were collected a hourly, 2-hourly and 6-hourly intervals, depending on the month, for transmitter

and receiver sites. In addition, meteorological measurements along the propagation path were recorded from a small fishing boat.

As discussed earlier, the complex processes occurring at the air/ocean boundary demand sophisticated measurements for detailed description. Since the necessary degree of sophistication is beyond the capability of field meteorologists simple "bulk" meteorological observations were purposely made.

The evaporation duct height models of Jeske, Rotheram, and Davidson are initiated with these data. The resultant δ for each model is then associated with a propagation pathloss measured directly and at the same time as the meteorological measurement. The duct height and its associated pathloss are then compared to a theoretical distribution as described by reference 4.

OBJECTIVE II

For the second objective, the "bulk".meteorological observations are used to drive each model to produce a plot of δ with time. Differences in computed δ between the three models are then compared for relative performance and sensitivity to "bulk" meteorological parameters.

OBJECTIVE III

To achieve the third objective, the propagation pathloss models of Rotheram and NOSC, hereafter referred to as the IREPS model, are employed.

Propagation pathloss calculations from the IREPS model are conducted in two steps. First, the Jeske evaporation duct height model is employed for determination of an n profile under neutral conditions. Neutral conditions are defined as those where the air-sea surface temperature difference is equal to zero. Secondly, using this piecewise linear n profile, numerical techniques are employed to calculate reflection coefficients. Numerical solutions of the fundamental equation of mode theory are then found using these reflection coefficients.

The Rotheram model for propagation loss also seeks to solve the fundamental equation of mode theory.

Differences of concern between the two models come from two factors.

1. The IREPS model assumes no effect from atmospheric stability on the propagation loss. Rotheram's model, on the other hand, includes a stability dependent effective earth's radius factor in the calculation of the standard radio horizon.

2. The IREPS model assumes a smooth earth surface, whereas the Rotheram model includes a root-mean-square sea roughness height (standard deviation of the sea surface from its mean level) in the computation of the attenuation value.

Each model is driven with the "bulk" meteorological observation as discussed earlier. The resultant propagation loss is compared to the observed propagation loss associated with the meteorological observation. A statistical distribution of propagation pathloss also is created for each model and

compared with the statistical distribution of observed pathloss values. This "smoothing" allows for comparison of theory without undue influence of "extreme" input parameters.

OBJECTIVE IV

To achieve the fourth objective, the IREPS model is driven with the "bulk" meteorological observations. An estimated pathloss value is generated for a fixed range of 35.2 km, the range between the transmitter and receiver for pathloss observations. This estimated pathloss is in turn used to calculate an estimated maximum detection range. By using the observed pathloss value, an "inferred" actual maximum detection range is calculated. A comparison of estimated maximum range and inferred maximum range is made to determine detection range error boundaries for use in assessing IREPS reliability.

RESULTS

CURRENT TECHNIQUE EVALUATION

The first two objectives of this report are met by considering the evaporation duct height models of Jeske, Rotheram, and Davidson and employing the meteorological observations for all four time periods and both island locations. Because of the frequency of November meteorological data and because relative model performance is similar for each period, the November data will be used in all comparisons unless stated otherwise. Also, for comparative purposes, a reasonable δ will be defined as 40 meters or less.

Figures 1 and 3* illustrate δ as a function of time for each model. General trends of synoptic and diurnal height fluctuations are nearly equally produced by all three models, but performance on individual data shows a great variance and will account, in some part, for the extremes in comparison data. For example, identical meteorological inputs produced δ of 16, 30, and 1189 meters by the models of Jeske, Rotheram, and Davidson, respectively. The discontinuity in the Davidson δ data is due to the model's inability to handle certain meteorological combinations and will be explained later. Table 1 displays the basic statistics for the evaporation duct height as calculated by the models of Jeske, Rotheram and Davidson.

Davidson's Model

Of the three evaporation duct height models, Davidson's is the most variable. Duct heights ranged between 0 and 1189 meters with a mean δ of 22.7 meters. Correlation with the δ of Jeske and Rotheram is 0.273 and 0.365, respectively.

For stable conditions, air temperature warmer than sea surface temperature, an air-sea temperature difference of 1°C coupled with low humidities and wind velocities, is sufficient to produce an unrealistic δ. For example, for Rh = 55% and U = 1 m sec^{-1}, δ = 242 meters. Increasing Rh by 10% or U by 1 m sec^{-1}, decreases δ to 14 and 49 meters, respectively.

For neutral conditions and U = 1 m sec^{-1}, the model failed to produce a δ as a function of Rh and T_a. For example, if $T_a = T_s$ = 19°C and Rh = 62%, the model fails. If $T_a = T_s$ = 15°C, the model will fail when Rh = 51%. For U > 1 m sec^{-1}, the model produces realistic δ regardless of Rh.

For unstable conditions, air temperature colder than sea surface temperatures, and U = 1 m sec^{-1}, the model fails to produce a δ regardless of Rh. If U > 1 m sec^{-1}, however, reasonable duct heights were obtained in all cases.

For the November observation period, the meteorological conditions necessary to produce an unrealistic δ or a model failure occurred 3.3 and 14.0 percent of the time, respectively. For the February period, the percentages

---

*All figures and tables are placed at the end of the report.

are 5.1 and 13.6; for the April period, the percentages are 21.1 and 25.0; and for the August period, unrealistic δ or failure percentages are 26.7 and 14.0, respectively.

Rotheram's Model

Rotheram's evaporation duct height model is much less variable with individual meteorological data than that of Davidson. δ varies from 0 to 253 meters with a mean δ of 11.5 meters. δ correlations with Jeske's and Davidson's models are 0.93 and 0.365, respectively.

As with Davidson's model, stable conditions coupled with low humidities and wind velocities are sufficient to produce an unrealistic δ, but not to the extent shown by the Davidson model. For example, with T_a = 20°C, T_s = 19°C, Rh = 78%, and U = 3 m sec^{-1}, δ = 182 and 327 meters for Rotheram and Davidson, respectively.

For neutral and unstable conditions, the model never failed to produce a δ, regardless of the meteorological parameters.

The meteorological conditions necessary to produce an unrealistic δ occurred 8.4, 5.7, 4.9, and 3.9 percent of the time for February, April, August, and November, respectively.

Jeske's Model

Jeske's evaporation duct height model was the *least sensitive* to individual data. δ varies between 0 and 134 meters with a mean δ of 10.7 meters.

In all stability cases, Jeske's model fails to produce a δ only when U = 0. This occurred 3.4, 5.7, 0, and 0 percent of the time for February, April, August, and November, respectively.

The Jeske model behaves very similar to that of Rotheram. For stable conditions, low humidities and wind velocities produce unrealistic δ, but not to the extent shown by Rotheram. For example, if T_a = 20°C, T_s = 19°C, Rh = 78%, and U = 3 m sec^{-1}, the δ = 80 and 182 meters for Jeske and Rotheram, respectively.

Meteorological conditions necessary to produce an unrealistic δ occurred 11.8, 38.4, 52.1, and 2.0 percent of the time for February, April, August, and November, respectively.

For neutral and unstable conditions, reasonable δ were obtained 100 percent of the time regardless of the meteorological parameters, except for U = 0, as previously discussed.

PERFORMANCE, METEOROLOGICAL INPUT, AND COMPUTATION COMPARISONS

Because of the extreme complexity of measuring δ directly, actual δ values were not obtained during the observation period. Therefore, the duct heights calculated by each model are compared to a theoretical distribution of

δ as a function of pathloss, as discussed in reference 4. Figures 4 through 15 show the distribution of calculated δ versus observed pathloss at four frequencies for each duct height model. Superimposed on each diagram is the theoretical dependence of δ with pathloss.

From visual inspection, there appears to be no significant difference in the performance of the three models. While there is general agreement with the theoretical curves for each frequency, there exists a great variability within the individual data points, with the greatest variability occurring at low duct heights.

A mean pathloss error is created by taking the mean difference between observed and theoretical pathloss for each calculated duct height. The mean pathloss error as a function of δ and frequency is shown in figures 16 through 19. Again, no significant difference exists between the duct height models. Compared to theoretical pathloss values, there appears to be less than or equal to a 10-dB error for each model except for ducts less than 7 meters, where all three models show an inferred overestimated pathloss.

While all three models show a mean statistical agreement with present theory, model sensitivities to combinations of meteorological parameters produce an extreme variation of δ. The assumption of "bulk" meteorological parameters being sufficient for accurate individual δ determination is called into suspicion. It is seen that a T_s variation of just 1°C can produce totally different duct heights. Under normal operations, meteorological personnel are unable to measure the sea surface temperature to an accuracy of 1°C. In addition, given the influences of a ship's superstructure and operations such as launching aircraft, the other parameters of T_a, Rh, and U are equally difficult to measure to an accuracy required by any model.

The needed accuracy of meteorological inputs also calls into question the assumption of horizontal atmospheric homogeneity. Any synoptic or mesoscale circulation that would lead to horizontal homogeneity would also tend to produce neutral or stable conditions. It is seen that all models display their greatest sensitivities within the stable regimes. For unstable regimes, it is not unrealistic to observe both temporal and spatial meteorological parameter fluctuations greater than that required by the models. The pathloss errors experienced between observed and inferred pathlosses clearly reflect a desirability to consider atmospheric inhomogeneities over the propagation path. Current operational propagation models are incapable of addressing this topic, however. An extremely expensive and difficult research and development effort would be needed to collect and analyze data and to develop new propagation algorithms. Also, it is operationally impractical to sample the atmosphere in detail sufficient to adequately describe the propagation path.

COMPARISON AND EVALUATION OF PATHLOSS MODELS

The third objective of this report is to compare and evaluate the propagation loss models of Rotheram and IREPS.

Figures 20 through 29 are scatter plots of calculated pathloss from the models of Rotheram and IREPS versus the observed pathloss for the November observation period. Tables 2 and 3 display the basic statistics for pathlosses as observed and calculated by the pathloss models of IREPS and Rotheram.

At the L-band frequency, the standard deviations of observed, IREPS, and Rotheram pathloss are 3.5 dB, 4.0 dB, and 11.0 dB, respectively. As the frequency increases, the standard deviation of all three pathlosses increases, with the Rotheram standard deviation increasing most rapidly. At the KA-band frequency, the observed, IREPS, and Rotheram pathloss standard deviations are 5.6 dB, 15.7 dB, and 24.8 dB, respectively.

The correlation between the IREPS and Rotheram pathloss models is high for frequencies of X-band and below. For example, at S-band, the correlation between pathlosses is 0.93. At frequencies above X-band, however, the correlation falls to zero. This can be explained by the IREPS model not considering surface roughness, which becomes increasingly important with high frequencies.

The correlation between both model pathlosses and the observed pathloss increases from 0.35 at L-band to 0.59 at X-band, but again falls to zero at KA-band frequency. This is expected, however, since both models were developed to operate below 20 GHz, thereby eliminating consideration of atmospheric EM wave absorption.

Figures 30 through 34 show the cumulative percent occurrence of observed pathloss with the pathlosses calculated by Rotheram and IREPS as a function of frequency. The general trends of the curves taken together with the statistical summary demonstrate the statistical agreement with theory, but as with the evaporation duct height models, a large variance in individual data leads to discrepancies between model performance and observational data. Investigation of time periods other than November show similar statistical trends and model variabilities.

Statistically, the IREPS modeled pathloss is less variable than the Rotheram modeled pathloss, and therefore more closely represents the pathloss distribution as observed. Since a major input to the model is δ , and Jeske's duct height model employed by the IREPS pathloss model was the least variable, this is expected.

The correlation of the IREPS calculated pathloss to observed pathloss reaches a maximum at approximately 10 GHz, but is poor above this frequency. At higher frequencies, where surface roughness should influence the pathloss models, the correlation between both IREPS and Rotheram's pathloss models output and observed pathloss is not significantly sufficient to justify inclusion of a surface roughness parameter as defined by Rotheram.

MAXIMUM DETECTION ERROR DETERMINATION

The final objective of this report is to determine a maximum radar detection range prediction error for the IREPS propagation model.

Figures 35 through 39 are scatter plots for the estimated maximum detection range calculated by the IREPS model versus an inferred maximum detection range based upon an observed pathloss over the measurement range. Both estimated and inferred maximum detection ranges are based on a maximum free space detection range of 185 km.

Both calculated and inferred maximum detection ranges vary greatly because of the previously demonstrated sensitivity of δ to meteorological param-

eters, and the sensitivity of the propagation models height-gain function relationship to δ. Figure 40 is an example of the height-gain maximization curves used to extrapolate an inferred detection range from an observed pathloss, and illustrates the height-gain function, δ relationship. It becomes evident from the figure that a very small pathloss change, due to a change in δ, can cause an extreme change in maximum inferred detection range.

Correlations between calculated and inferred maximum detection ranges varied from a -0.02 at 3 GHz to a maximum of 0.5 at 10 GHz. By calculating the difference between computed and inferred maximum detection ranges, dividing this difference by the computed range, and then segregating these relative range errors into percent-error categories, a histogram of percent occurrence versus relative detection range error is derived. The histograms for each frequency band are displayed in figures 41 through 45. For L- and S-band frequencies that are not significantly affected by the evaporation duct, relative detection range errors of less than 50% occurred 98.1% and 90.7% of the time, respectively. For X-band frequencies, the relative detection range errors of less than 50% occur 57.0% of the time. At K-band, where the evaporation duct has the greatest influence in propagation, the IREPS model produces detection range errors of less than 50% only 30.8% of the time. Relative detection range errors were in excess of 100% 45.7 percent of the time. For the KA-band frequencies, the relative detection range errors of less than 50% increases to 62.4% of the time. This increase is to be expected, since once again the evaporation duct effect diminishes. The increase is not as dramatic as at lower frequencies, however, since atmospheric absorption, which is not modeled in the IREPS program, becomes a substantial factor in propagation. With the exception of the KA-band frequency, the IREPS model tends to underestimate a maximum detection range, with the greatest underestimation occurring at S-band frequencies.

Statistical analysis of the IREPS detection range software cannot be used to support the soundness of propagation theory as well as it did evaporation duct theory. The model's sensitivity to the evaporation duct height is vividly demonstrated by the frequency dependent detection range errors, but the ability of the model to perform when the influence of the evaporation duct height is greatest is poor.

For this reason, it becomes even more important to understand that the IREPS software is written to assess relative emitter systems performance, and not to produce an absolute propagation range value.

CONCLUSIONS

1. The evaporation duct height models of Jeske, Rotheram, and Davidson function equally well with reasonable duct heights calculated when considering the statistical average of meteorological inputs. When individual meteorological data points are considered, however, the three models show a wide fluctuation in outputs. The model of Jeske shows the most reasonable duct height for any particular meteorological situation, while the model of Davidson shows the greatest variance. Because of the equal functioning when considering statistical average, the model performance is more a function of the individual meteorological parameters than of any one technique of duct height calculation.

2. The meteorological observations taken by operational personnel are not of sufficient quality to insure proper duct height calculations when individual duct height predictions are desired.

3. The evaporation duct height is a major input to the propagation models of IREPS and Rotheram. Since individual duct heights show large variances, both models reflect large fluctuations in individual pathloss calculations. When considering statistical means in observational data, both models function reasonably well, with the IREPS model more closely representing observation. Since the IREPS model does not include a direct consideration of surface roughness as does Rotheram's model, but performs equally or slightly better within some frequency bands, the additional effort to model surface roughness does not appear to be justified.

4. A second consequence of the model's sensitivity to individual meteorological inputs involves a reasonable model performance when assuming atmospheric horizontal homogeneity. It is obvious that in regions of air mass boundaries, horizontal homogeneity is a poor assumption. It is shown that the models' sensitivities to meteorological inputs indicates a desirability for consideration of a heterogeneous atmosphere. Given the inability of meteorological personnel to make sufficiently accurate measurements, however, attempts to develop new theoretical techniques to allow more inputs for better horizontal resolution would prove counterproductive. Assuming model sensitivities to meteorological input could be overcome and new propagation algorithms for a heterogeneous atmosphere could be developed, the practicality and expense of operationally gathering sufficient quantities of input data to significantly reflect atmospheric conditions would be unreasonable. When considering all problems involved, the assumption of a homogeneous atmosphere for a fleet operational propagation model is realistic.

5. All previous conclusions indicate the theory behind calculation of duct height and pathloss values is statistically sound. For statistical studies of propagation phenomena or development of electromagnetic systems, both the IREPS and Rotheram models perform reasonably well and are accurate predictors. However, the use of the IREPS model for estimation of individual propagation ranges based upon an individual meteorological observation is suspect. At L-, S-, X-, KU-, and KA-band frequencies, the IREPS model produced median relative range errors of 5, 19, 40, 83, and 31 percent, respectively. The poorest performance of IREPS occurs at frequencies most affected by the evaporation duct.

RECOMMENDATIONS

1. Quality of individual meteorological observations needed as input to current state-of-the-art propagation models is insufficient. The quality can be improved by two methods:

   a. Improve the observational skills of the individual through further training, with emphasis on attention to established observational procedures.

   b. Develop a sensor system that can be deployed away from heating/cooling and turbulent effects created by the observation platform.

2. In the face of insufficient quality in observed meteorological data and the sensitivity of duct height models to these data, develop an entirely new duct height model using statistical techniques.

3. Current propagation models are based upon pathloss values created from assumed conditions of atmospheric absorption, atmosheric homogeneity, system noise, etc. Controlled experiments need to be designed to investigate the role of each assumption upon the actual pathloss over the propagation path.

4. Train fleet operators of the IREPS model in the limitations and recognition of situations in which the model's performance is marginal or poor.

5. Undertake further evaluation of the IREPS model by comparing a predicted range with an actual observed maximum detection range.

REFERENCES

1. Jeske, H, The State of Radar-range Prediction Over Sea, AGARD Conference Proceedings No. 70, Part II, 50.1-50.10, February 1971.

2. Rotheram, S, Radiowave Range Prediction Over the Sea in Evaporation Ducting Conditions, Marconi Research Laboratories Technical Report 77/37, Great Baddow, Chelmsford, CM2 N, November 1977.

3. Fairall, CW and KL Davidson, Evaporation Duct Measurements in the Mid Atlantic, Naval Postgraduate School Report 61-78-005, 15 August 1978.

4. Hitney, HV, Propagation Modeling in the Evaporation Duct, NELC/TR 1947, 1 April 1975.

5. Monin, AS and AM Obukhov, Basic Laws of Turbulent Mixing in the Ground Layer of the Atmoshere, Akad. Nauk. USSR Geofiz. Inst. Tr., (151), 163-187, 1954.

6. Richter, JH and HV Hitney, Antenna Heights for Optimum Utilization of the Oceanic Surface Evaporation Duct, Part III: Results from the Mediterranean Measurements, Naval Electronic Laboratory Center Technical Note 2569, 26 November 1973.

Table 1. Basic statistics for the evaporation duct height as calculated by the models of Jeske, Rotheram, and Davidson

Source	Mean (m)	Standard Deviation (m)	Maximum (m)	Minimum (m)
Jeske model	10.7	13.4	134.5	0.0
Rotheram model	11.5	23.7	353.7	0.0
Davidson model	22.7	96.8	1189.9	0.0

Correlation Matrix

	Jeske model	Rotheram model
Davidson Model	0.2729580	0.3655519
Jeske model		0.9281335

Table 2. Basic statistics for propagation pathloss as observed and calculated by the pathloss models of IREPS and Rotheram.

Frequency	Source	Mean (dB)	Standard Deviation (dB)	Maximum (dB)	Minimum (dB)
L-Band	Observation	151.7	3.5	158.3	132.2
(1.0426 GHz)	IREPS model	150.9	4.0	154.9	124.3
	Rotheram model	152.7	11.0	162.3	96.7
S-Band	Observation	159.0	6.7	170.0	129.2
(3.0075 GHz)	IREPS model	162.4	11.7	176.3	127.1
	Rotheram model	156.4	15.9	185.0	102.3
X-Band	Observation	151.4	11.6	187.9	125.9
(9.624 GHz)	IREPS model	157.6	12.3	183.0	136.4
	Rotheram model	158.5	19.3	227.2	108.0
KU-Band	Observation	152.9	8.0	179.9	137.4
(17.9648 GHz)	IREPS model	158.9	12.2	190.9	139.9
	Rotheram model	158.1	20.4	261.3	75.0
KA-Band	Observation	174.6	5.6	194.6	159.6
(37.44 GHz)	IREPS model	175.1	15.7	200.7	144.9
	Rotheram model	166.8	24.8	335.6	81.3

Table 3. Correlation of pathlosses as observed and calculated by the pathloss models of IREPS and Rotheram.

Frequency		Correlation Matrix	
		Observed	Rotheram model
L-Band (1.0426 GHz)	IREPS model	0.2782005	0.8666421
	Observed		0.3519613
S-Band (3.0075 GHz)	IREPS model	0.4819911	0.9366692
	Observed		0.4703576
X-Band (9.6240 GHz)	IREPS model	0.5373757	0.8569345
	Observed		0.5934058
KU-Band (17.9648 GHz)	IREPS model	0.1480623	0.3059226
	Observed		0.2303580
KA-Band (37.44 GHz)	IREPS model	-0.1457113	-0.0899832
	Observed		0.0553127

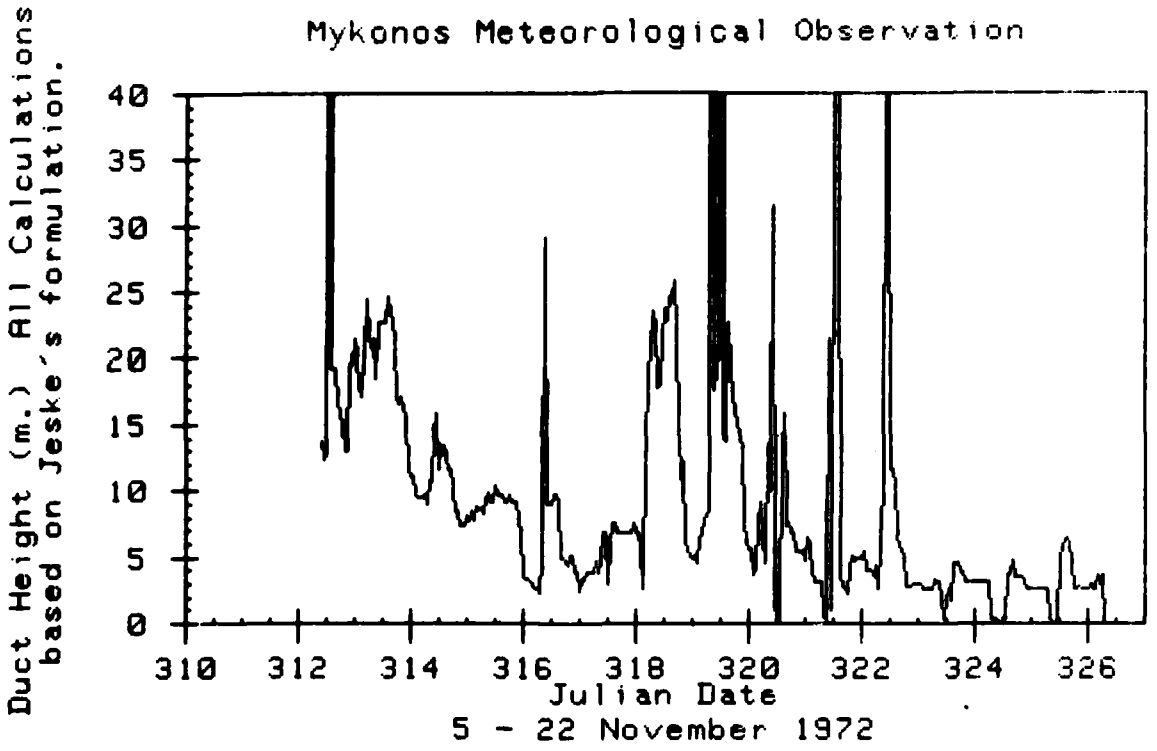

Figure 1. Jeske evaporation duct height versus time.

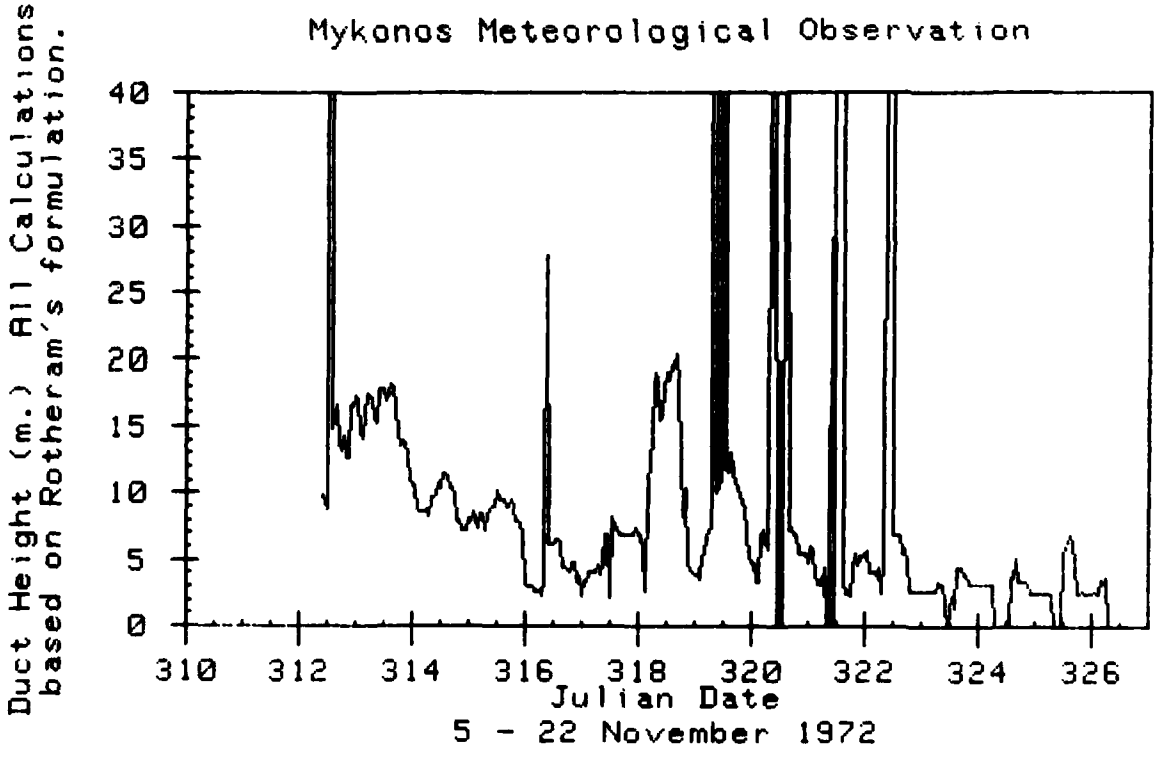

Figure 2. Rotheram evaporation duct height versus time.

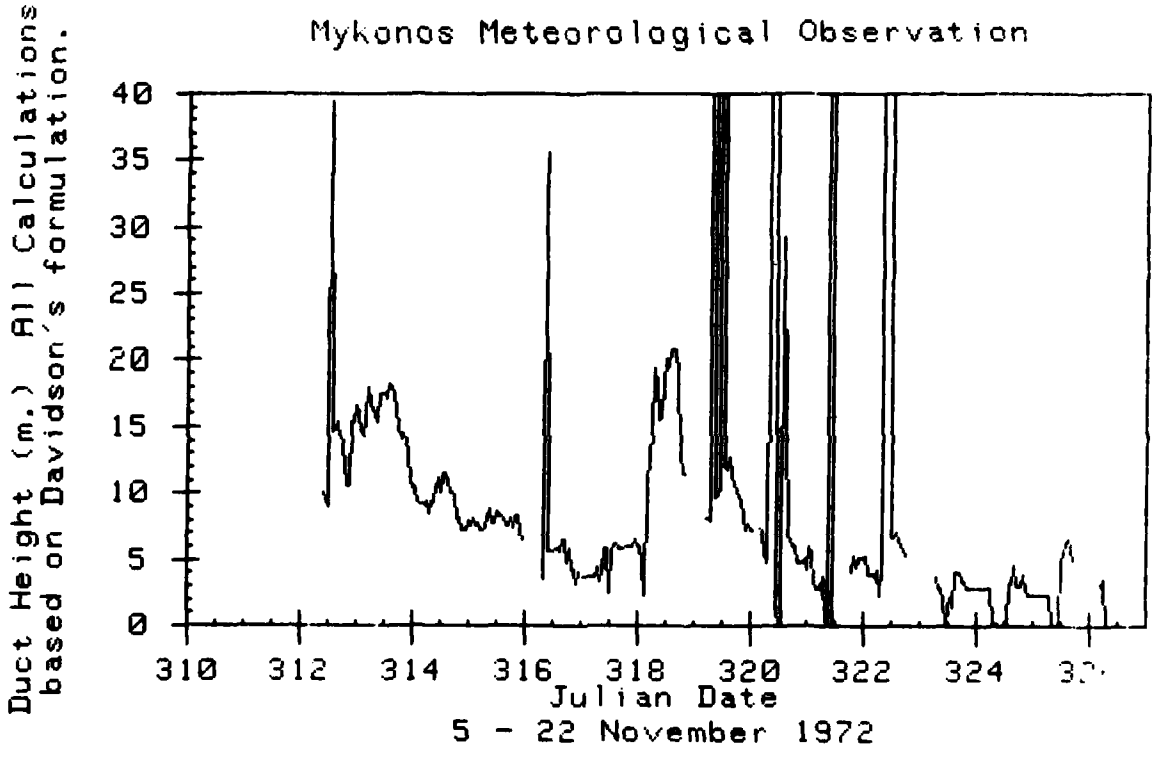

Figure 3. Davidson evaporation duct height versus time.

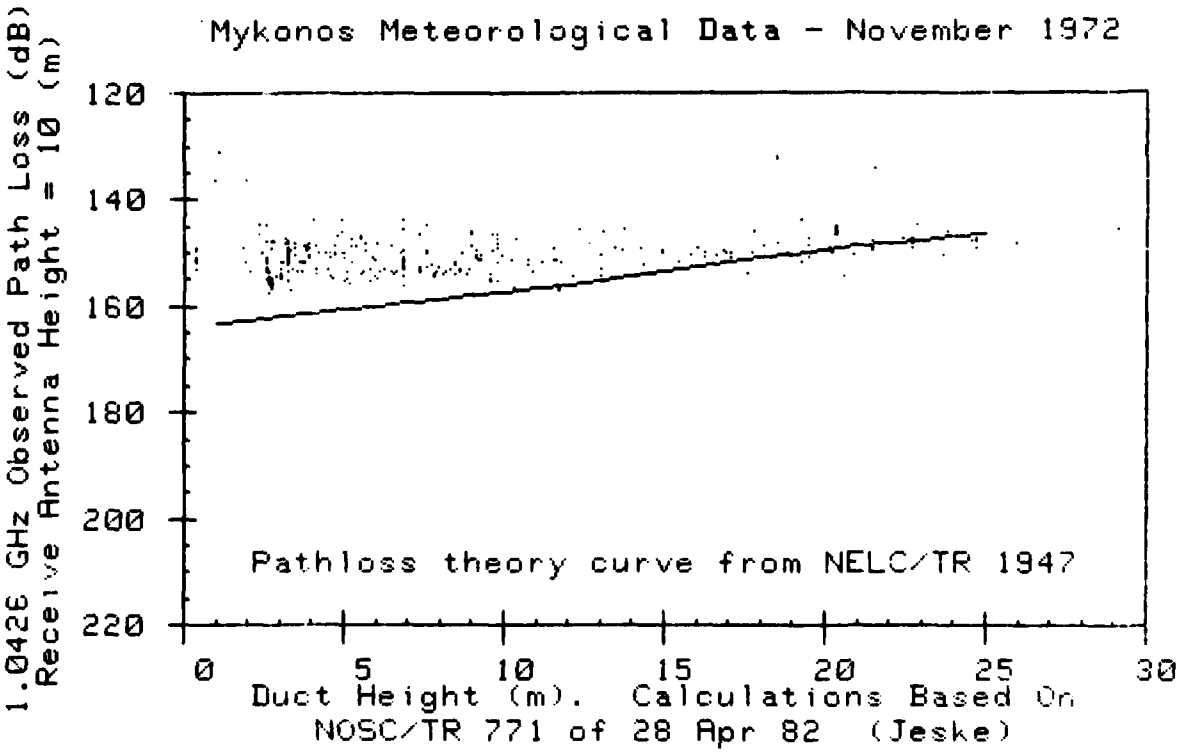

Figure 4. Jeske evaporation duct height versus L-band frequency observed pathloss.

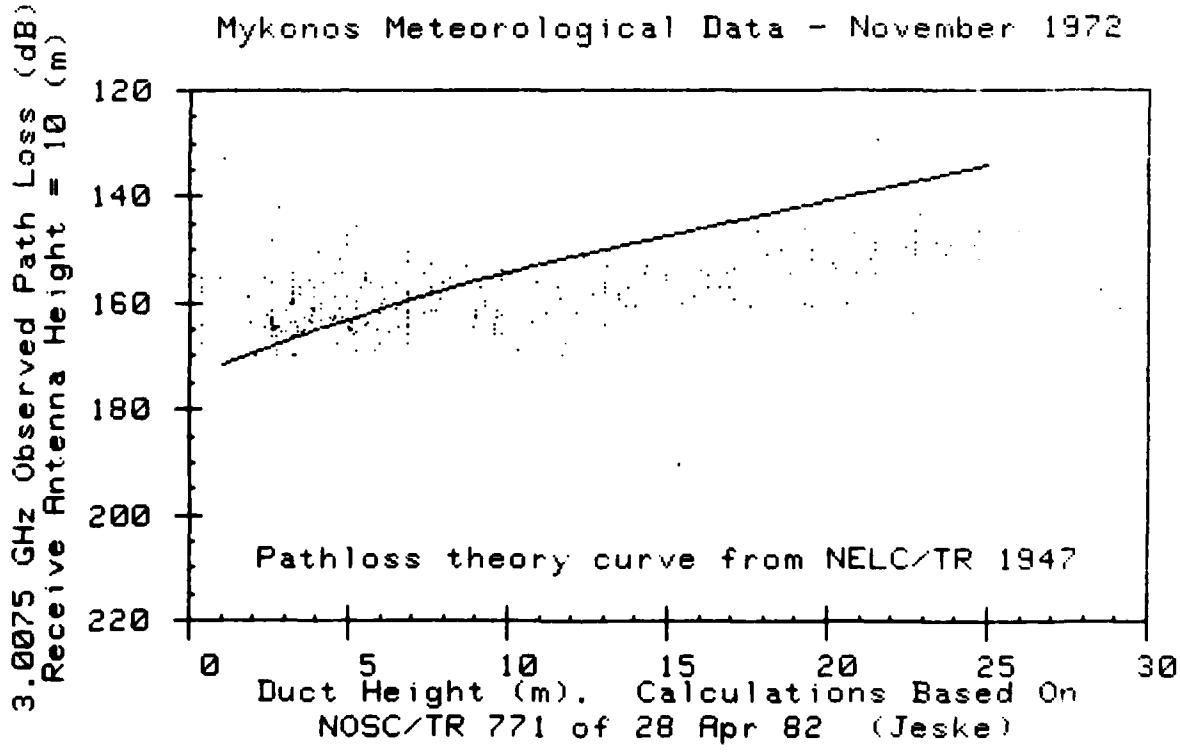

Figure 5. Jeske evaporation duct height versus S-band frequency observed pathloss.

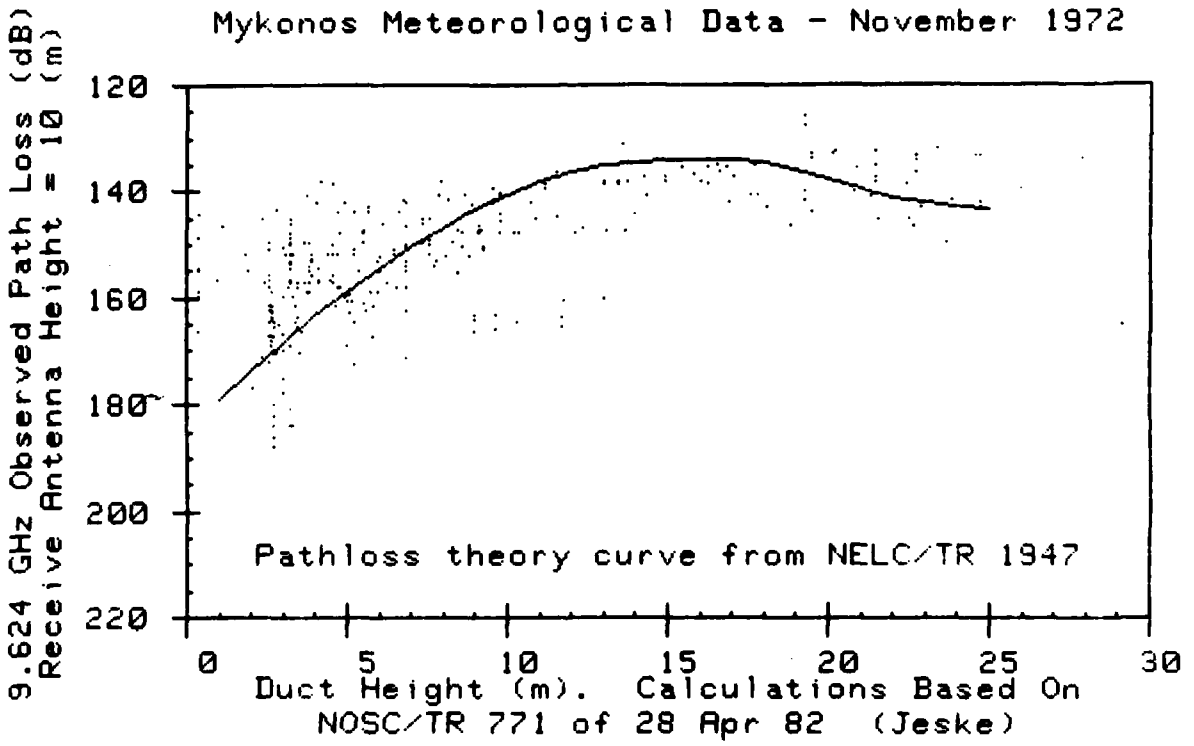

Figure 6. Jeske evaporation duct height versus X-band frequency observed pathloss.

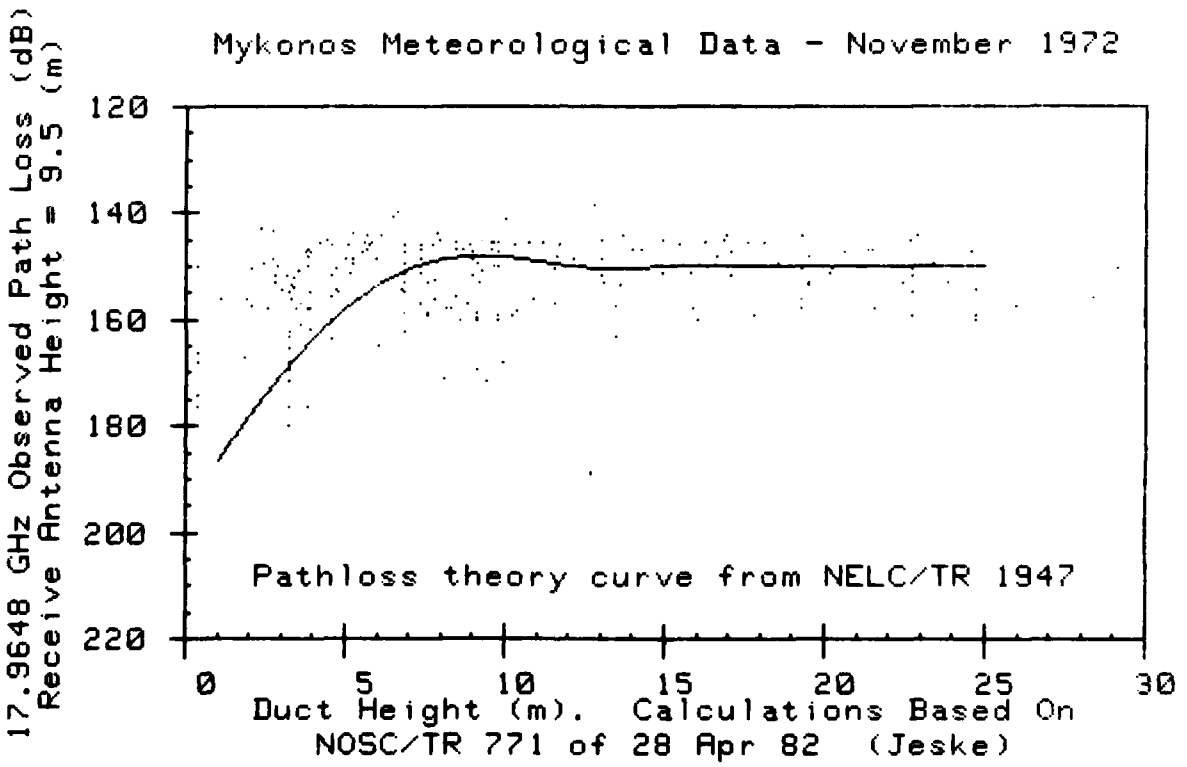

Figure 7. Jeske evaporation duct height versus KU-band frequency observed pathloss.

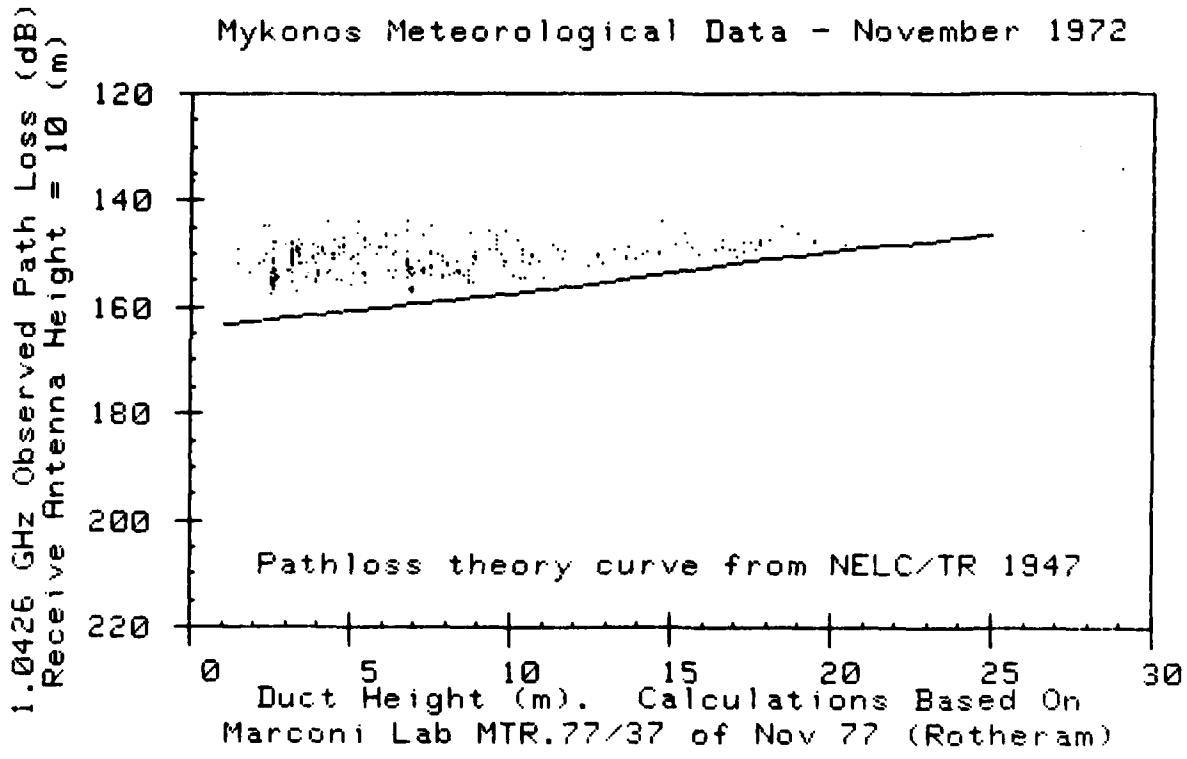

Figure 8. Rotheram evaporation duct height versus L-band frequency observed pathloss.

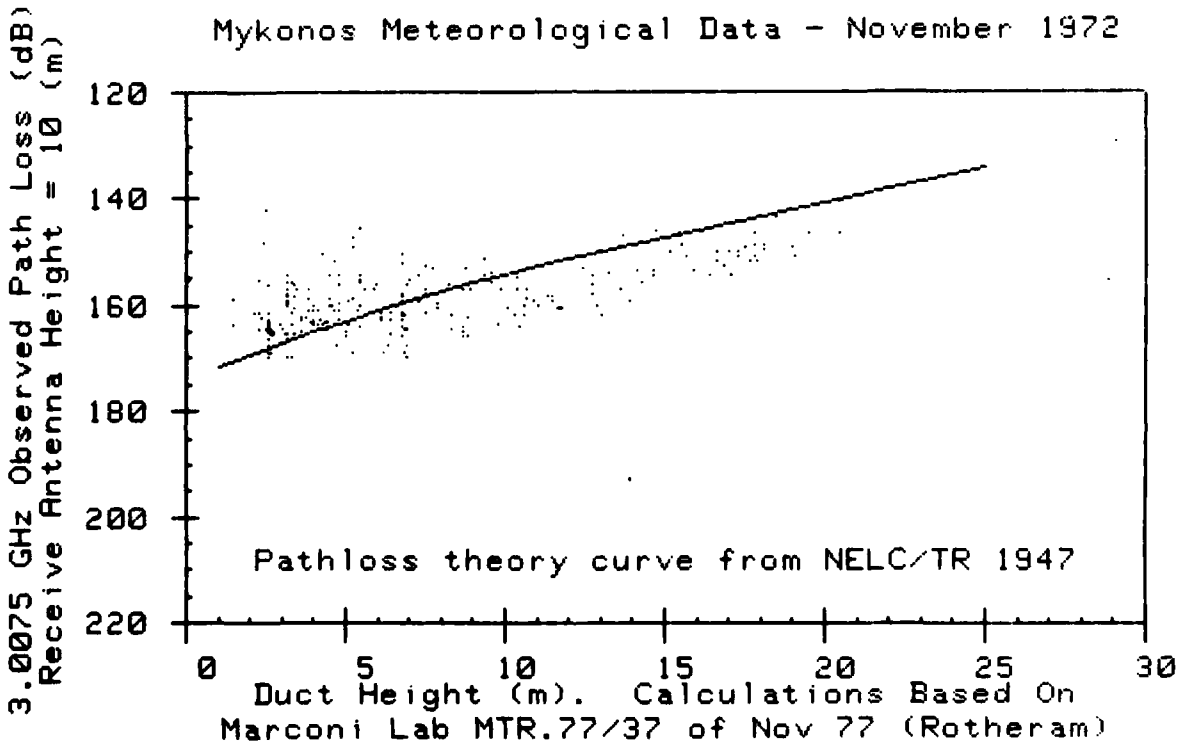

Figure 9. Rotheram evaporation duct height versus S-band frequency observed pathloss.

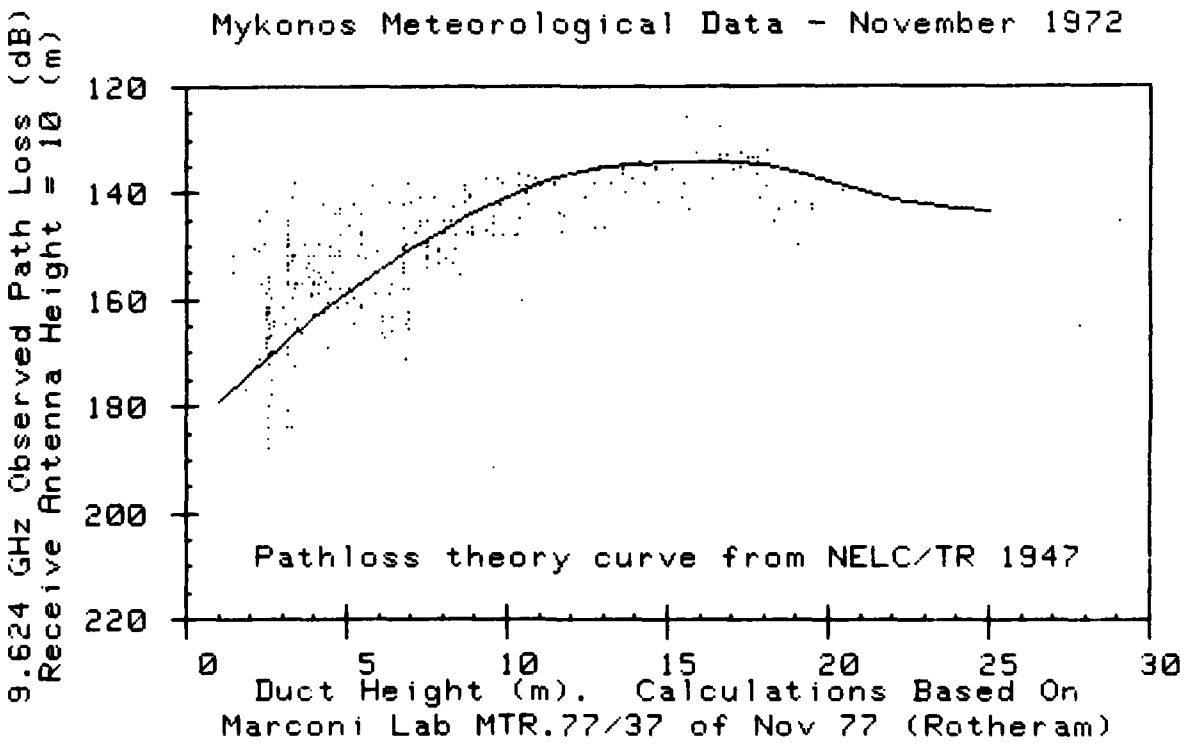

Figure 10. Rotheram evaporation duct height versus X-band frequency observed pathloss.

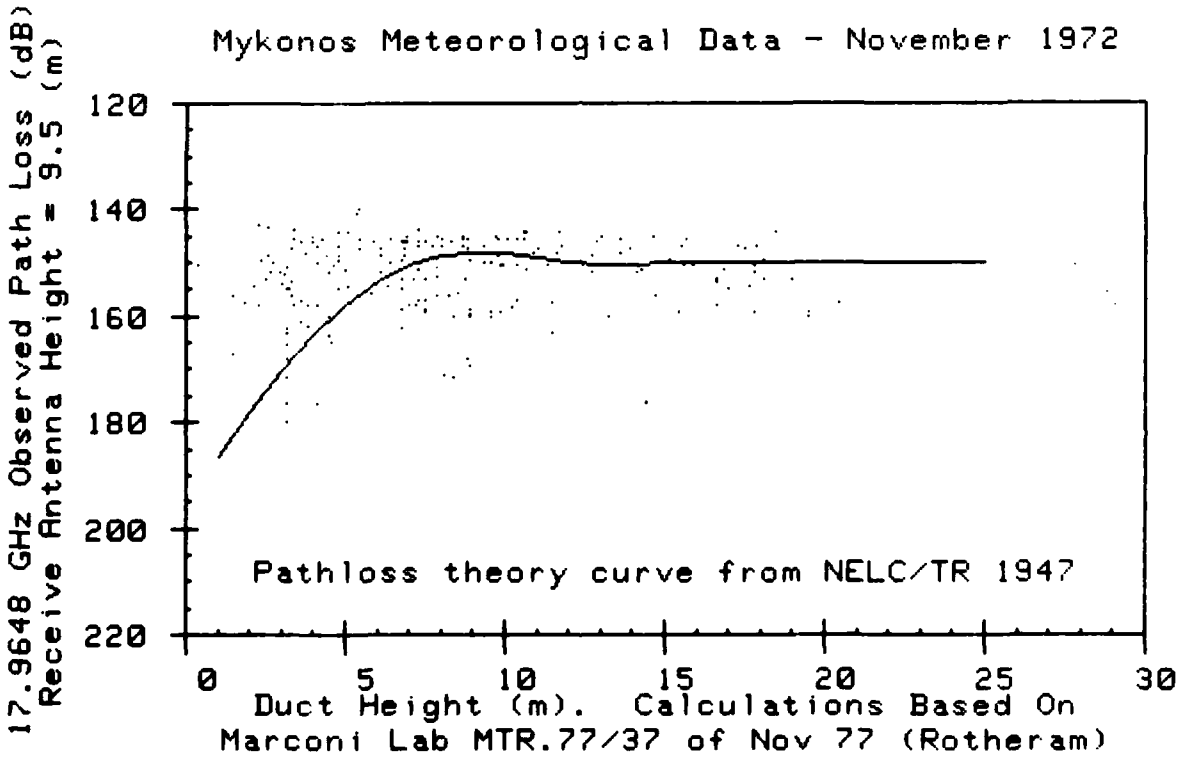

Figure 11. Rotheram evaporation duct height versus KU-band frequency observed pathloss.

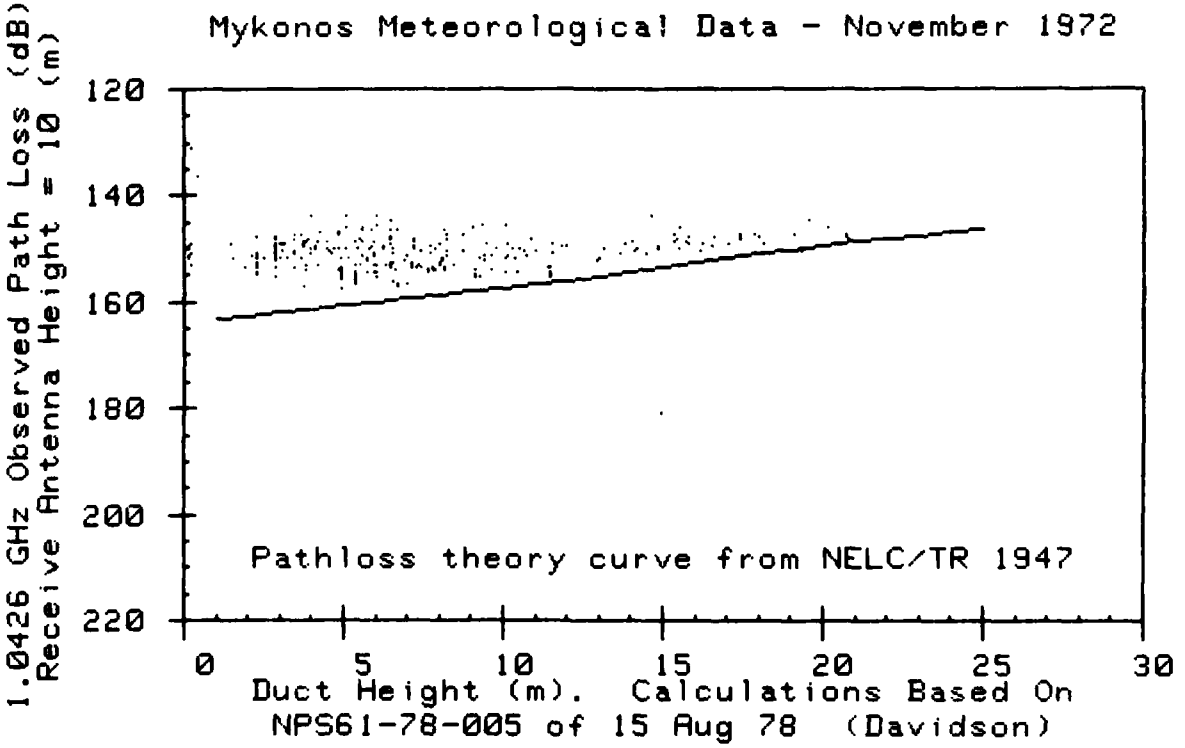

Figure 12. Davidson evaporation duct height versus L-band frequency observed pathloss.

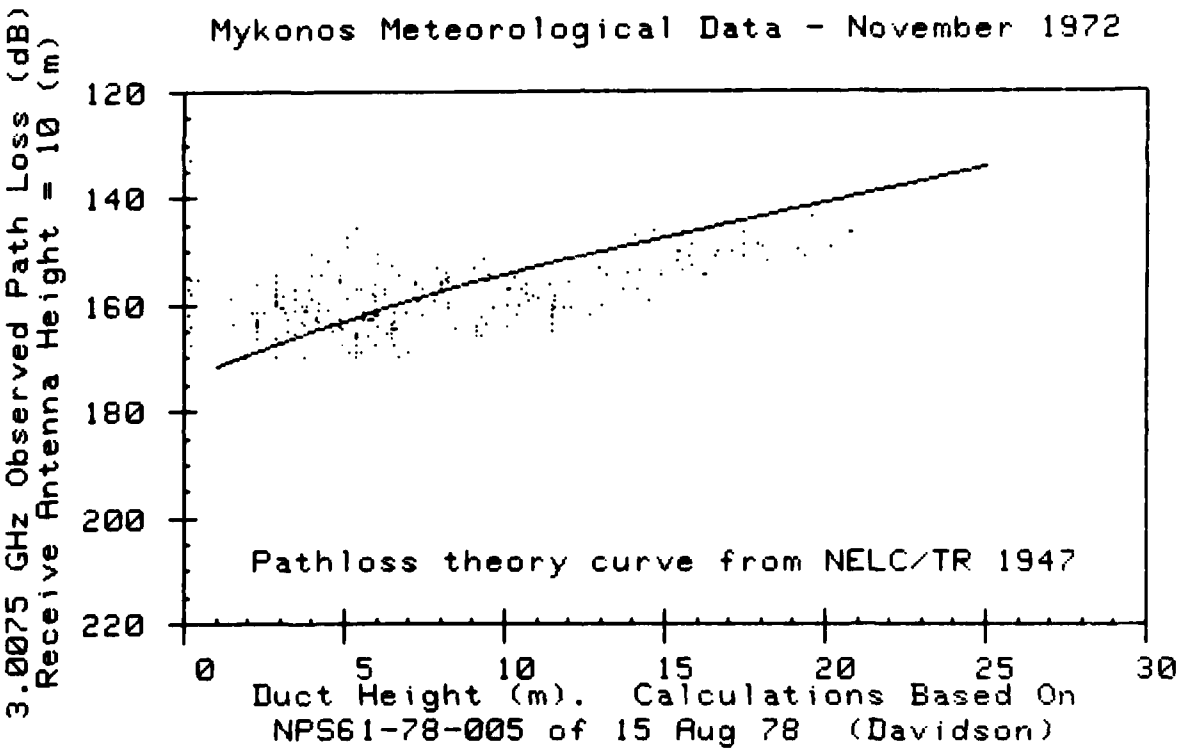

Figure 13. Davidson evaporation duct height versus S-band frequency observed pathloss.

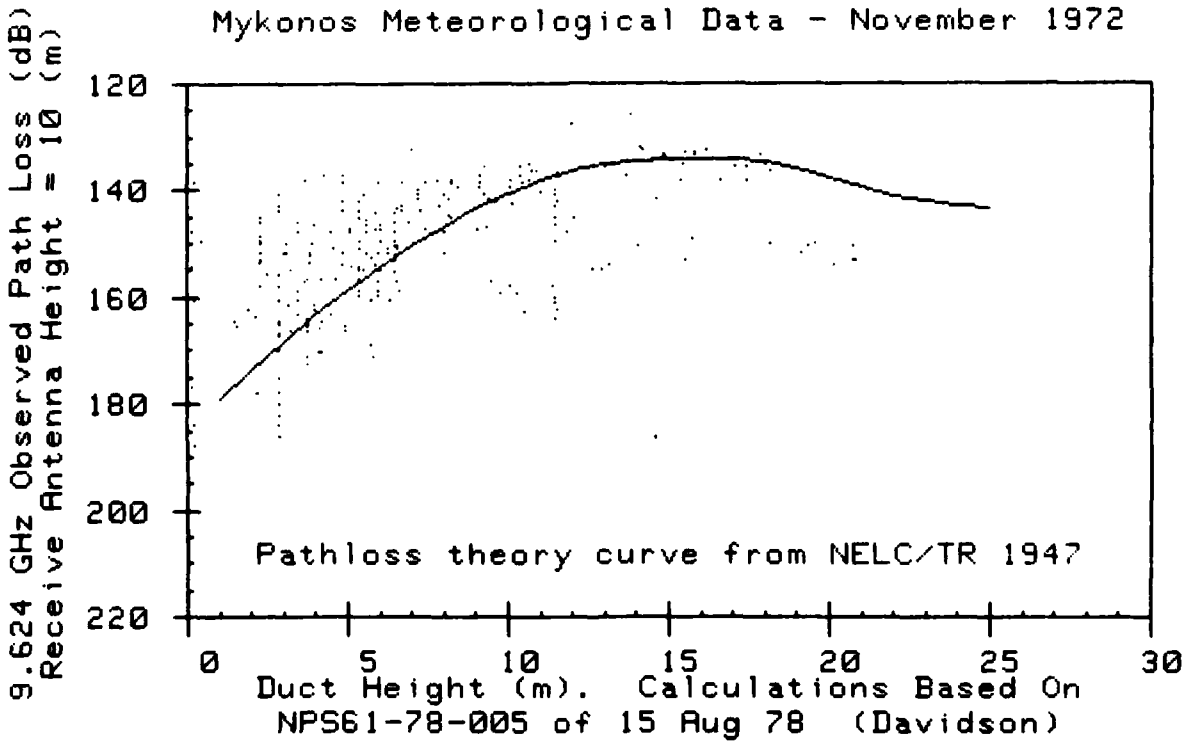

Figure 14. Davidson evaporation duct height versus X-band frequency observed pathloss.

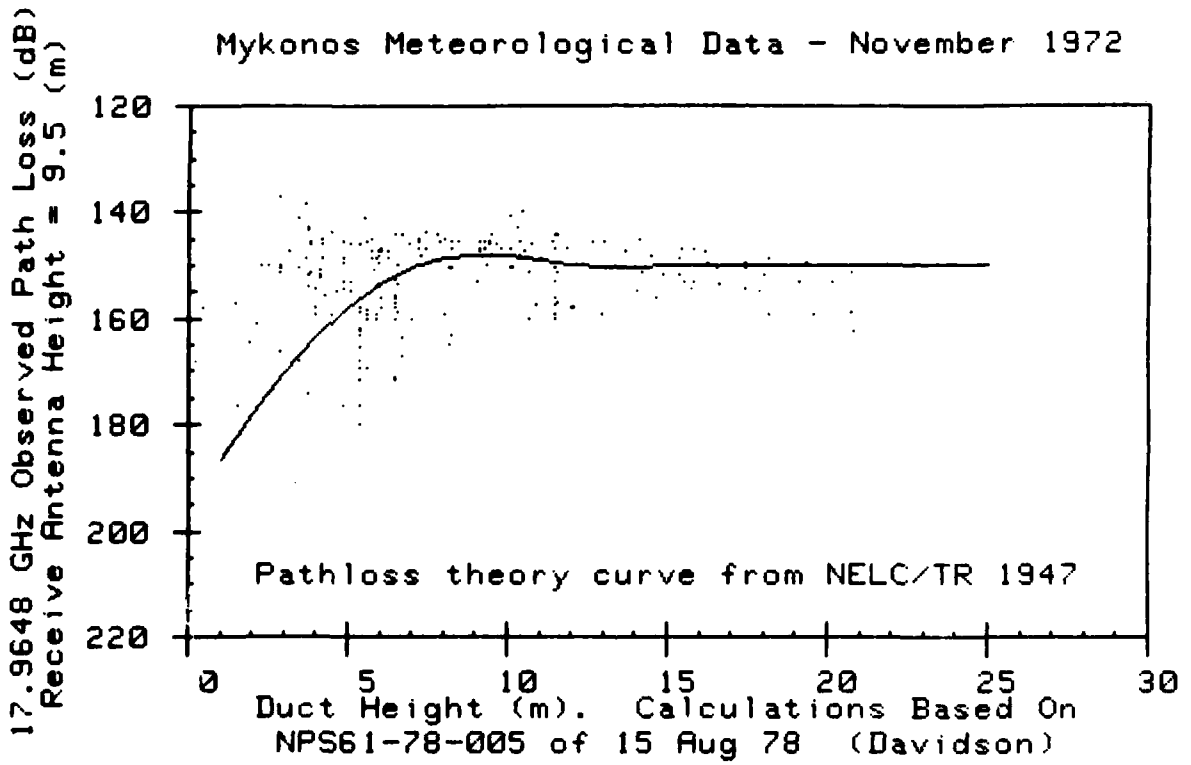

Figure 15. Davidson evaporation duct height versus KU-band frequency observed pathloss.

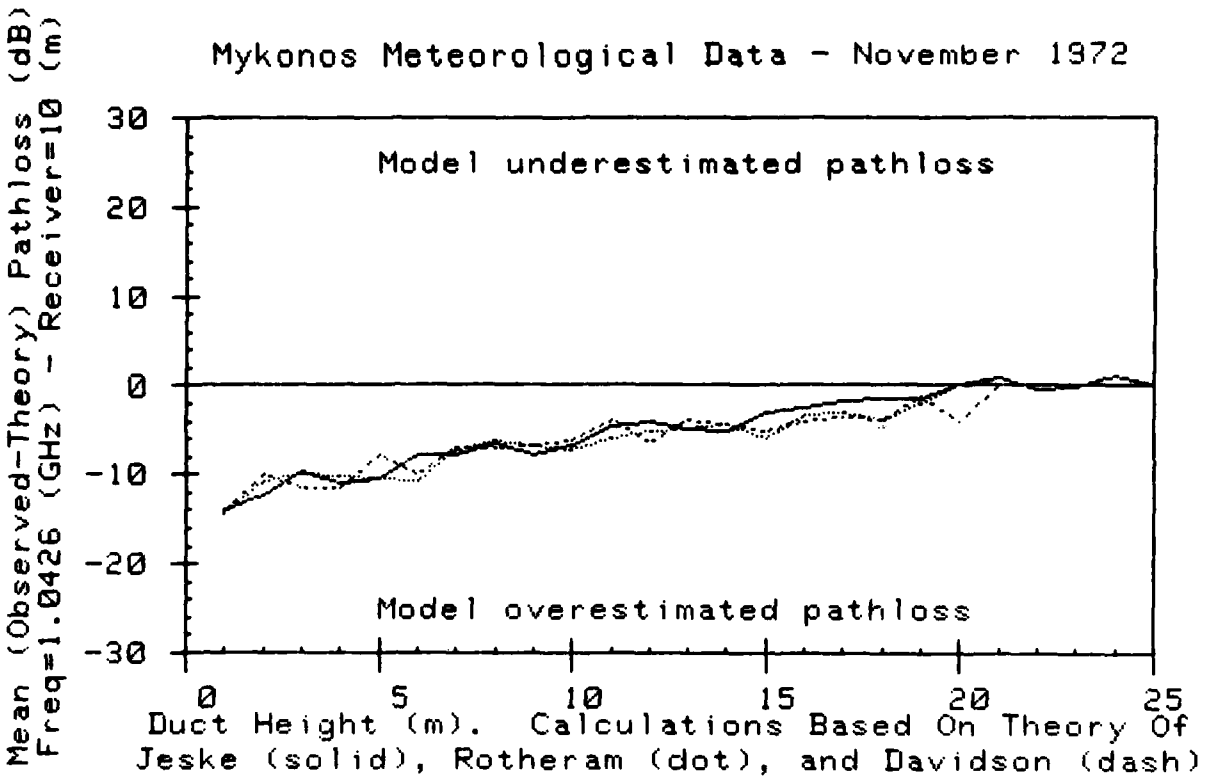

Figure 16. Three model evaporation duct height versus L-band frequency mean pathloss error.

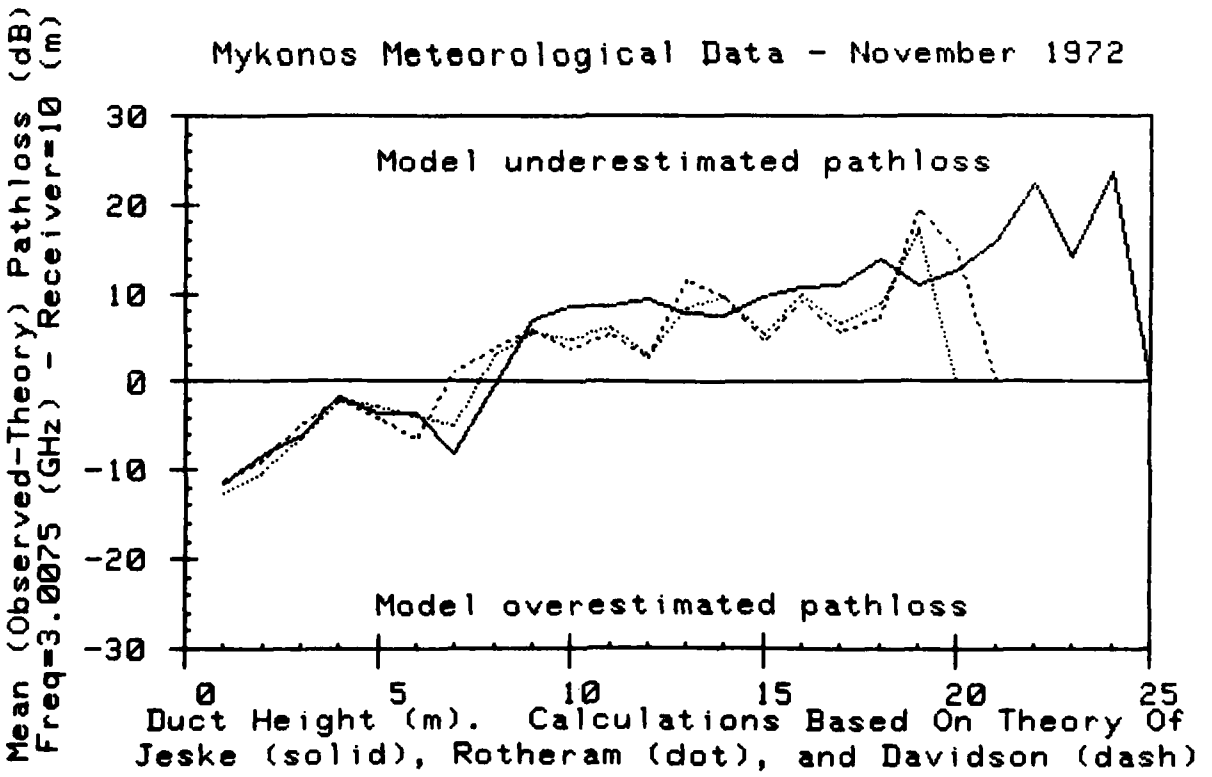

Figure 17. Three model evaporation duct height versus S-band frequency mean pathloss error.

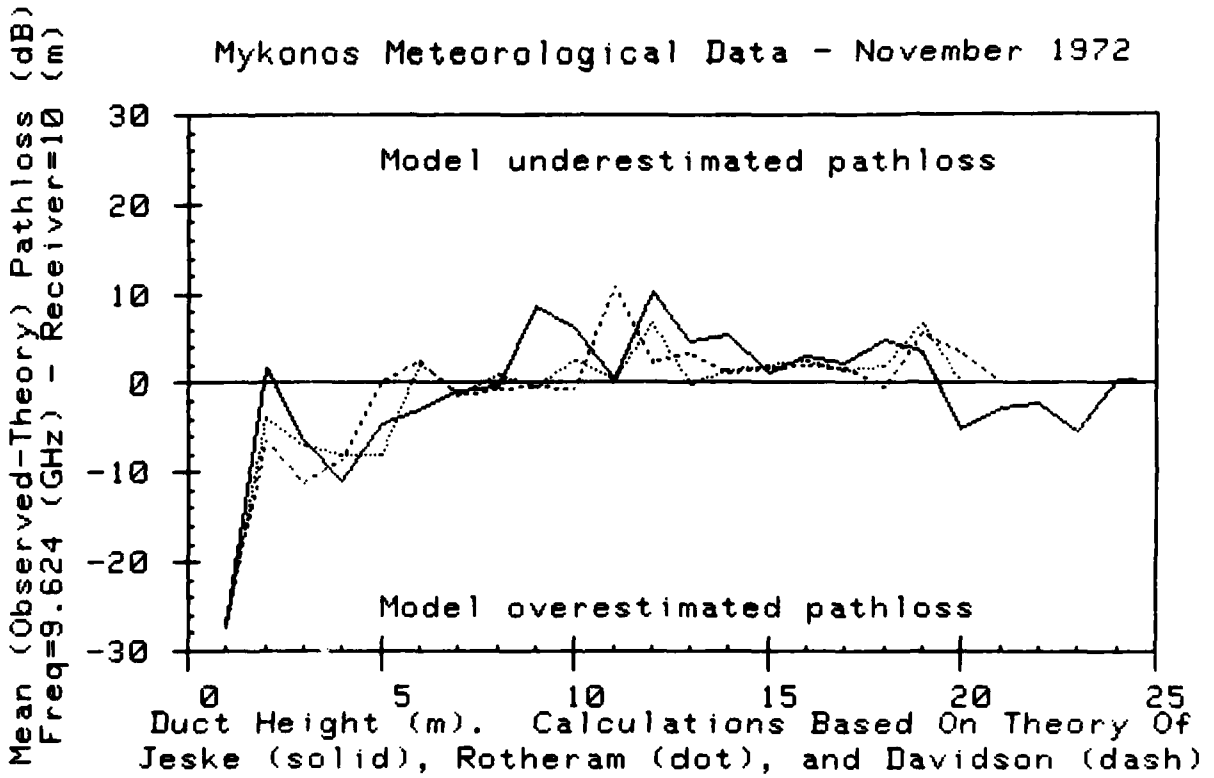

Figure 18. Three model evaporation duct height versus X-band frequency mean pathloss error.

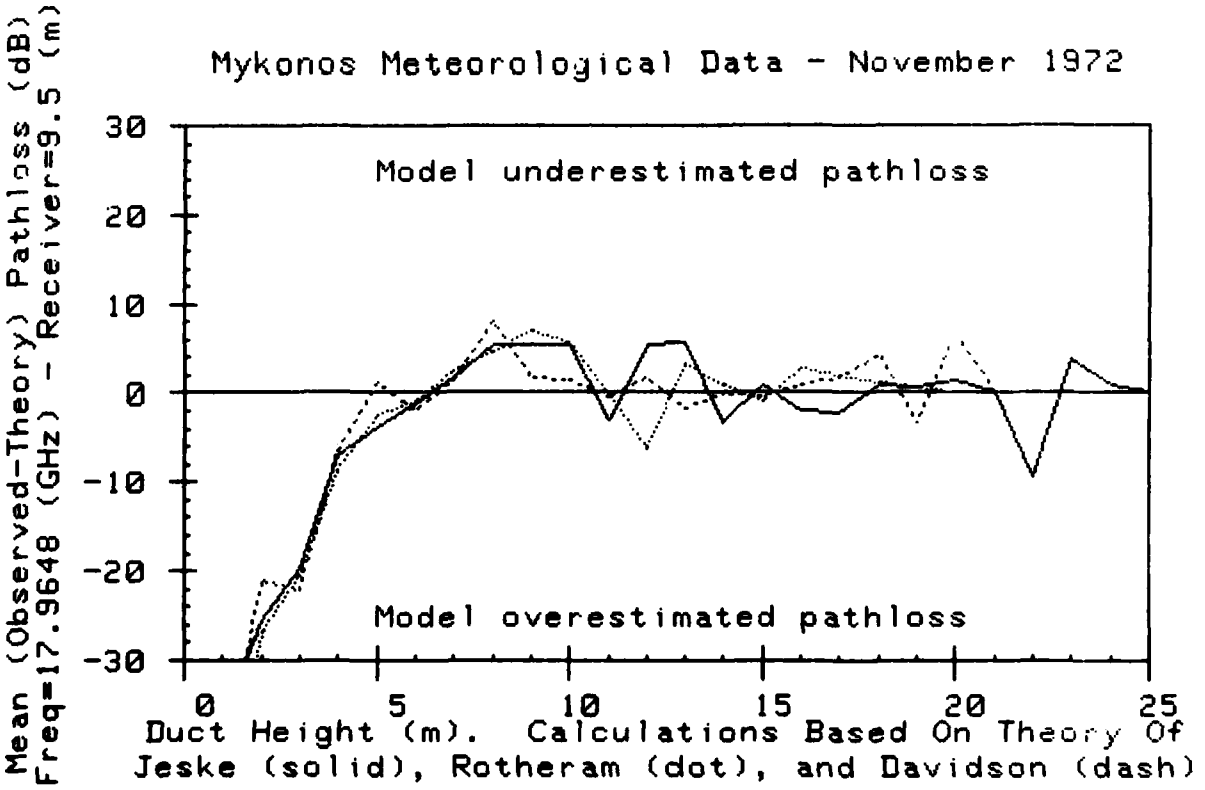

Figure 19. Three model evaporation duct height versus KU-band frequency mean pathloss error.

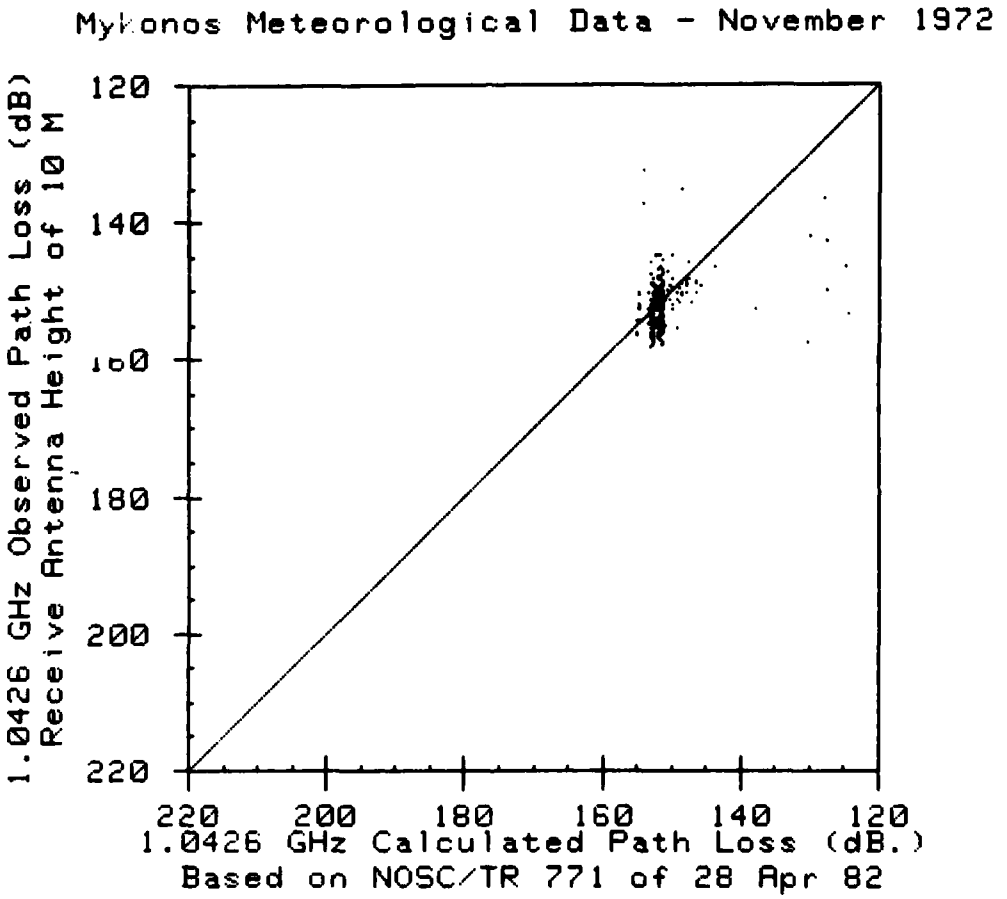

Figure 20. IREPS L-band frequency pathloss versus observed L-band frequency pathloss.

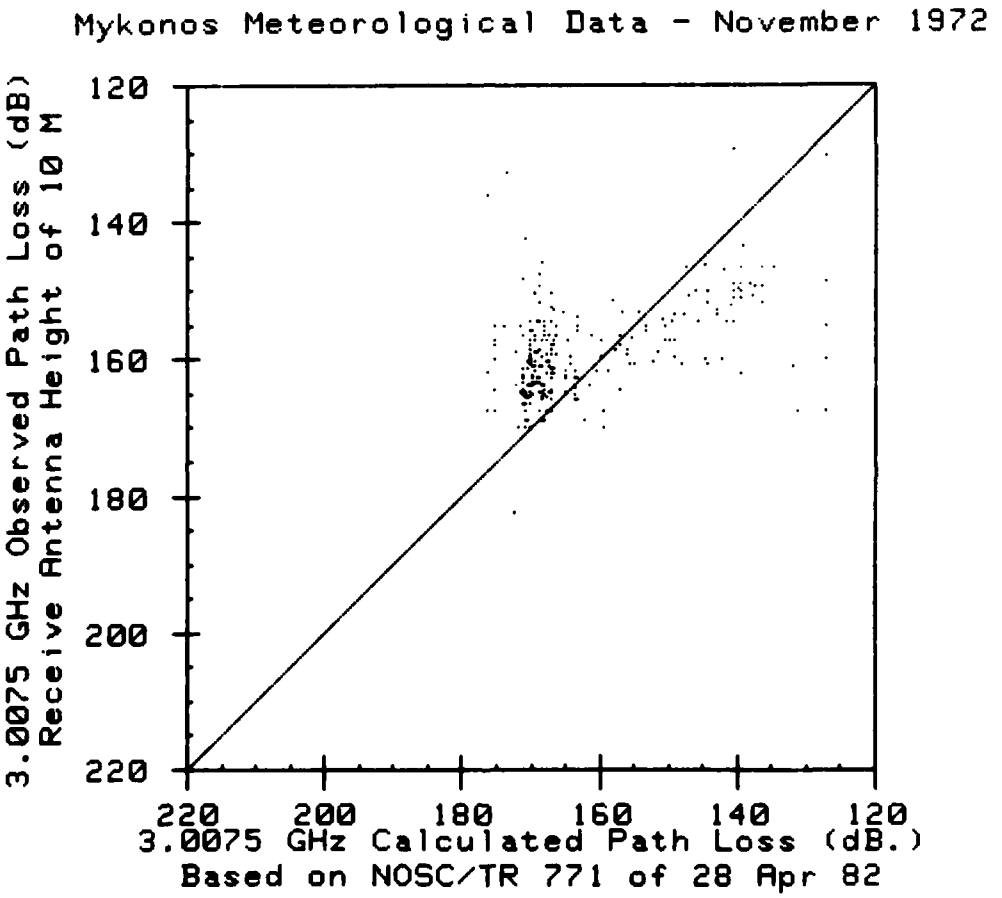

Figure 21. IREPS S-band frequency pathloss versus observed S-band frequency pathloss.

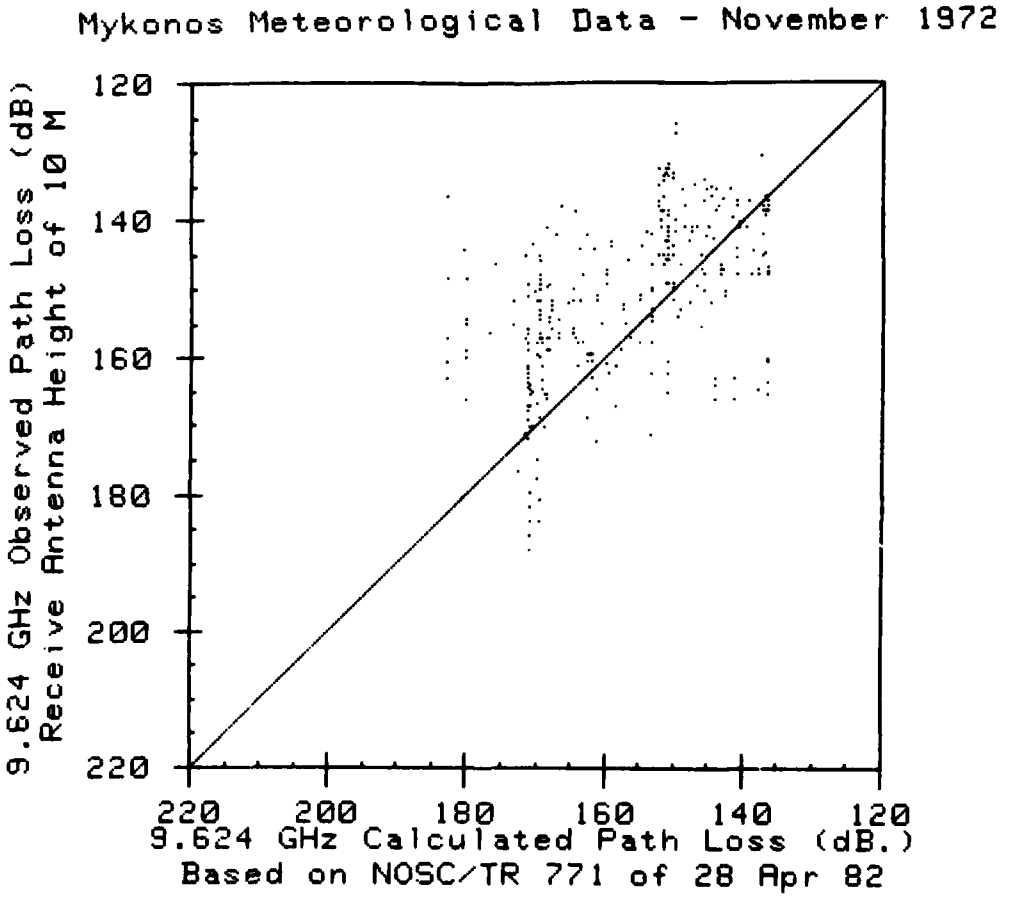

Figure 22. IREPS X-band frequency pathloss versus observed X-band frequency pathloss.

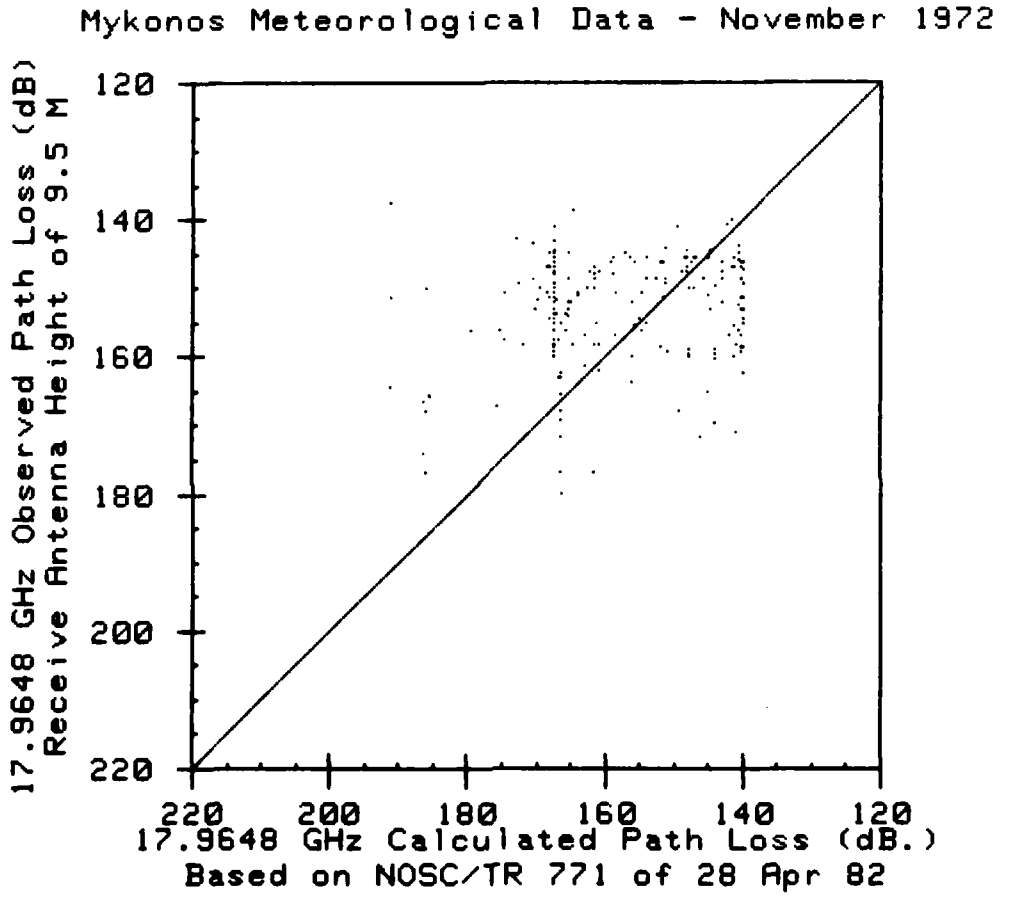

Figure 23. IREPS KU-band frequency pathloss versus observed KU-band frequency pathloss.

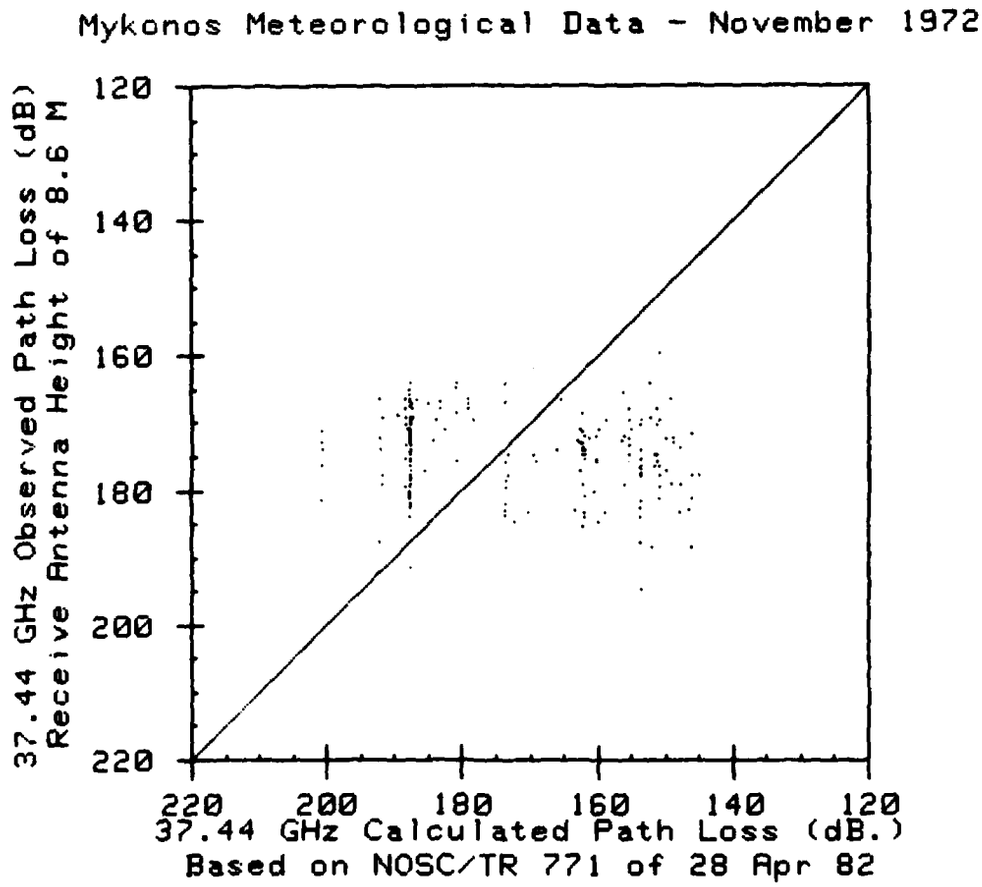

Figure 24. IREPS KA-band frequency pathloss versus observed KA-band frequency pathloss.

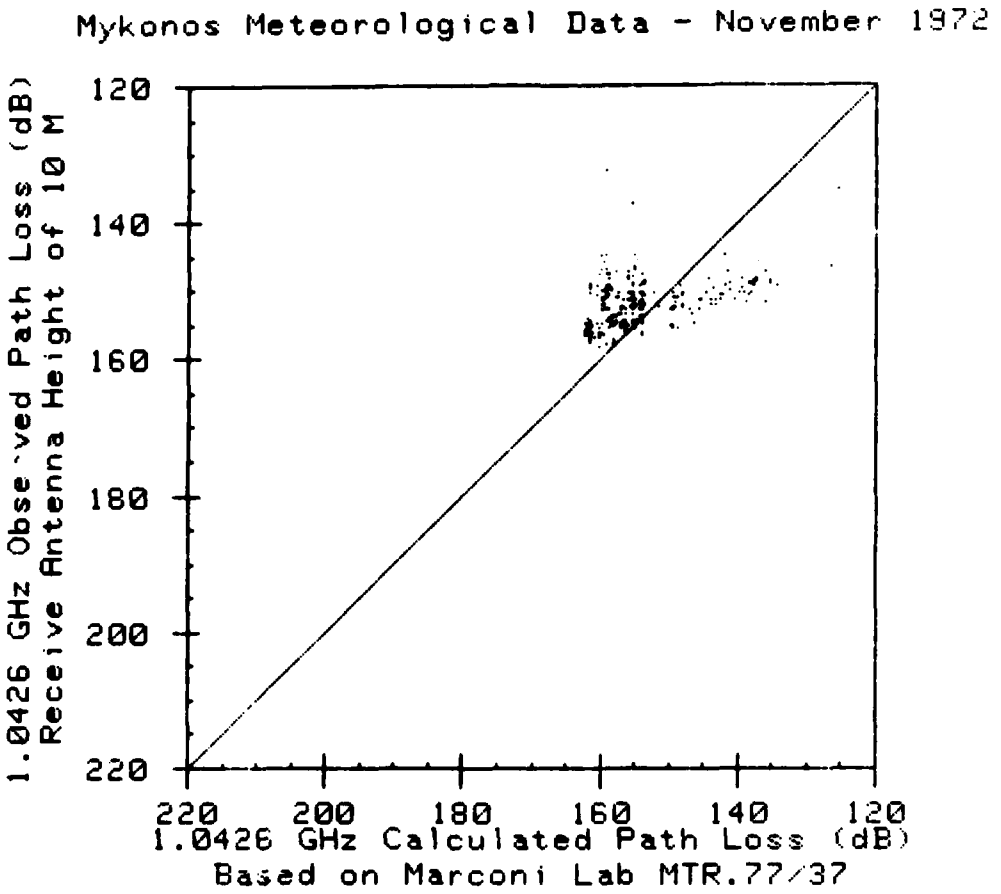

Figure 25. Rotheram L-band frequency pathloss versus observed L-band frequency pathloss.

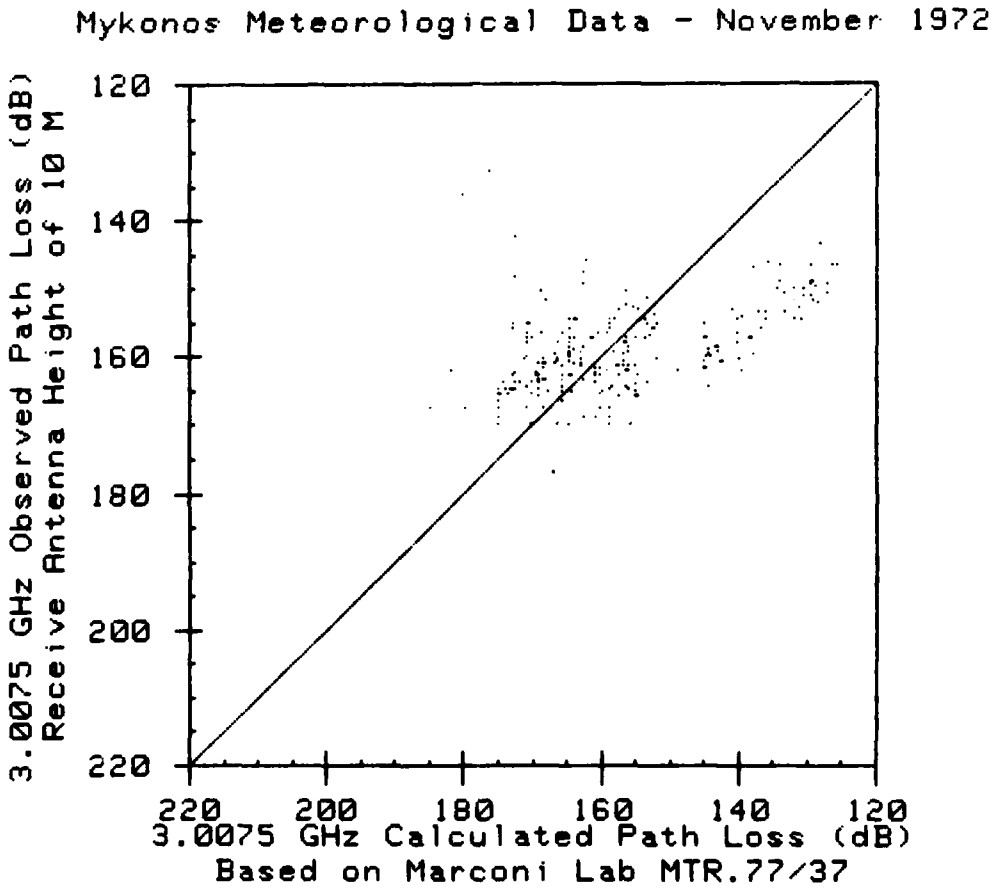

Figure 26. Rotheram S-band frequency pathloss versus observed S-band frequency pathloss.

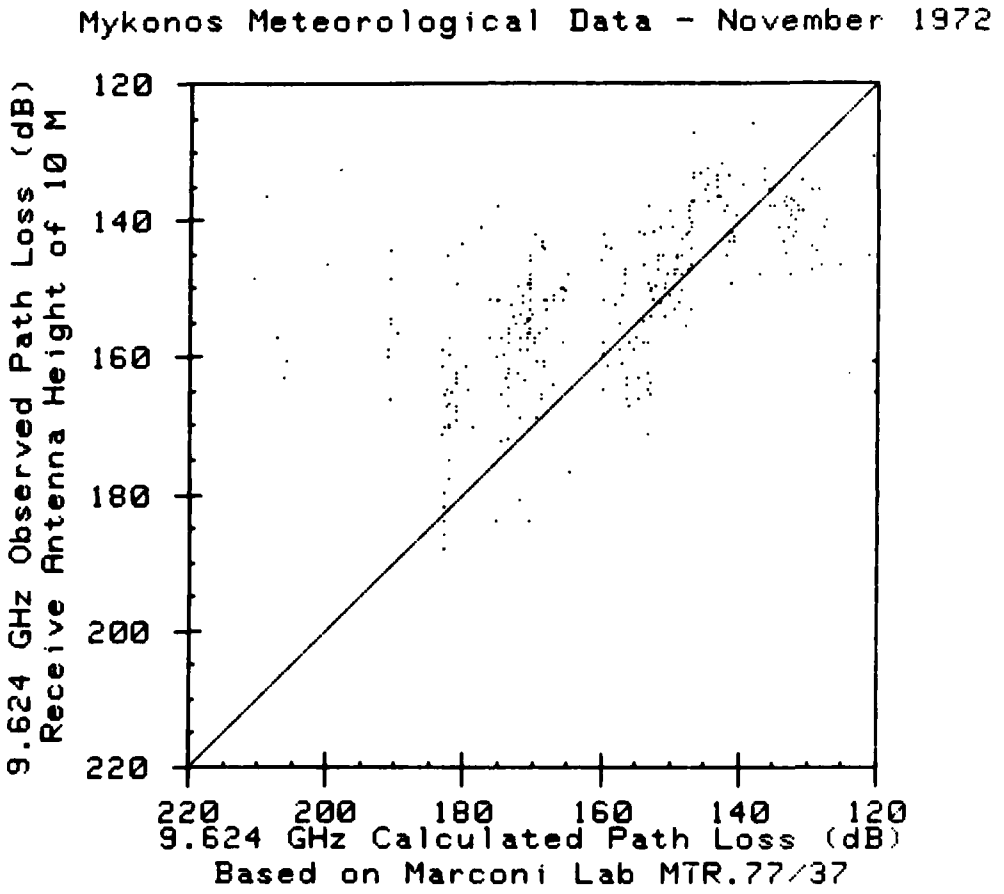

Figure 27. Rotheram X-band frequency pathloss versus observed X-band frequency pathloss.

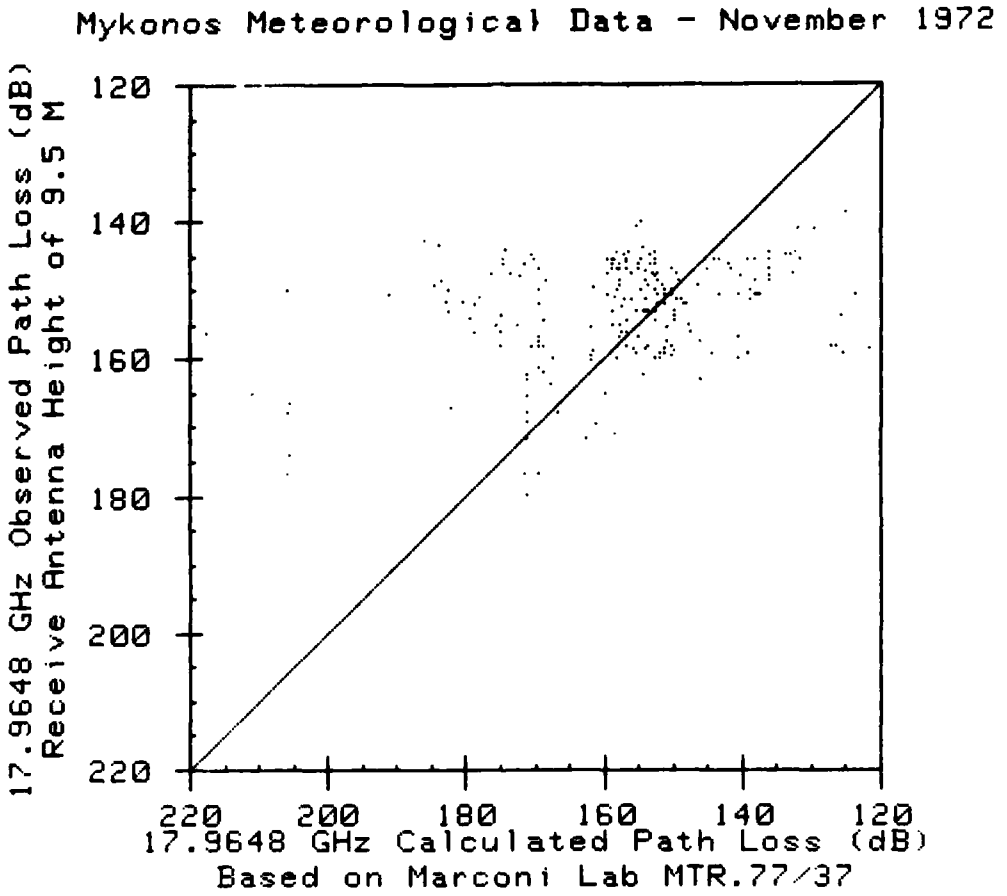

Figure 28. Hotneram KU-band frequency pathloss versus observed KU-band frequency pathloss.

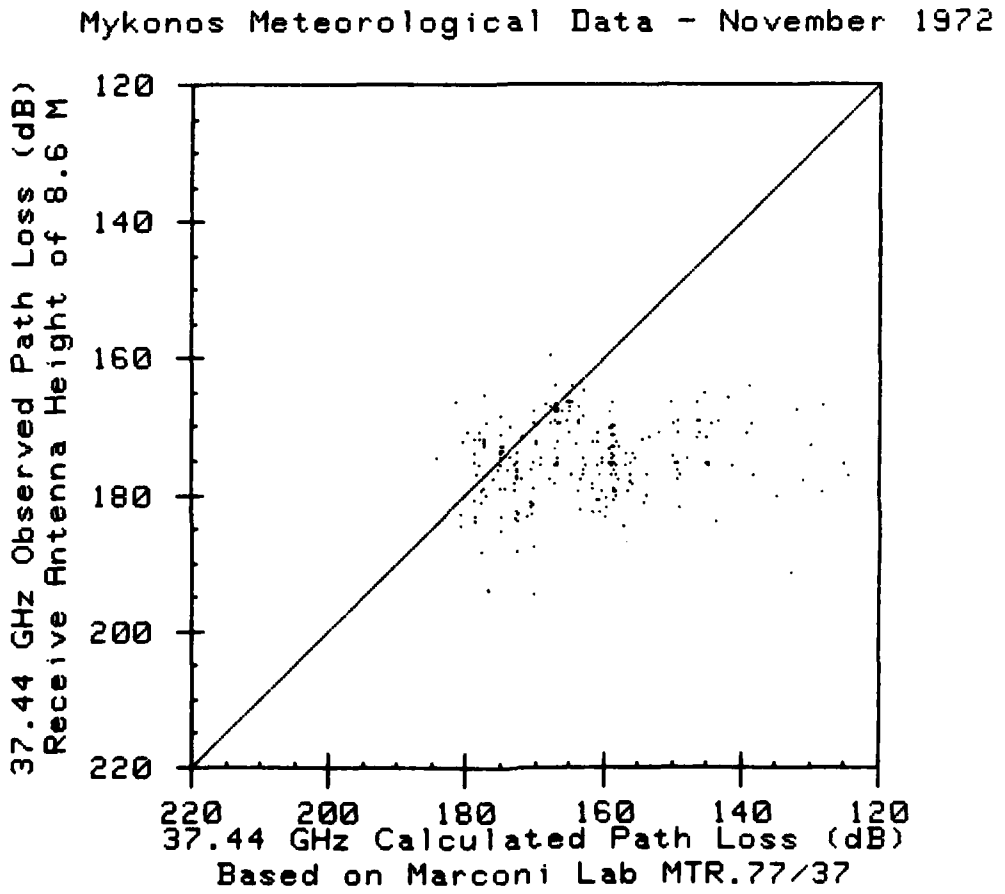

Figure 29. Rotheram KA-band frequency pathloss versus observed KA-band frequency pathloss.

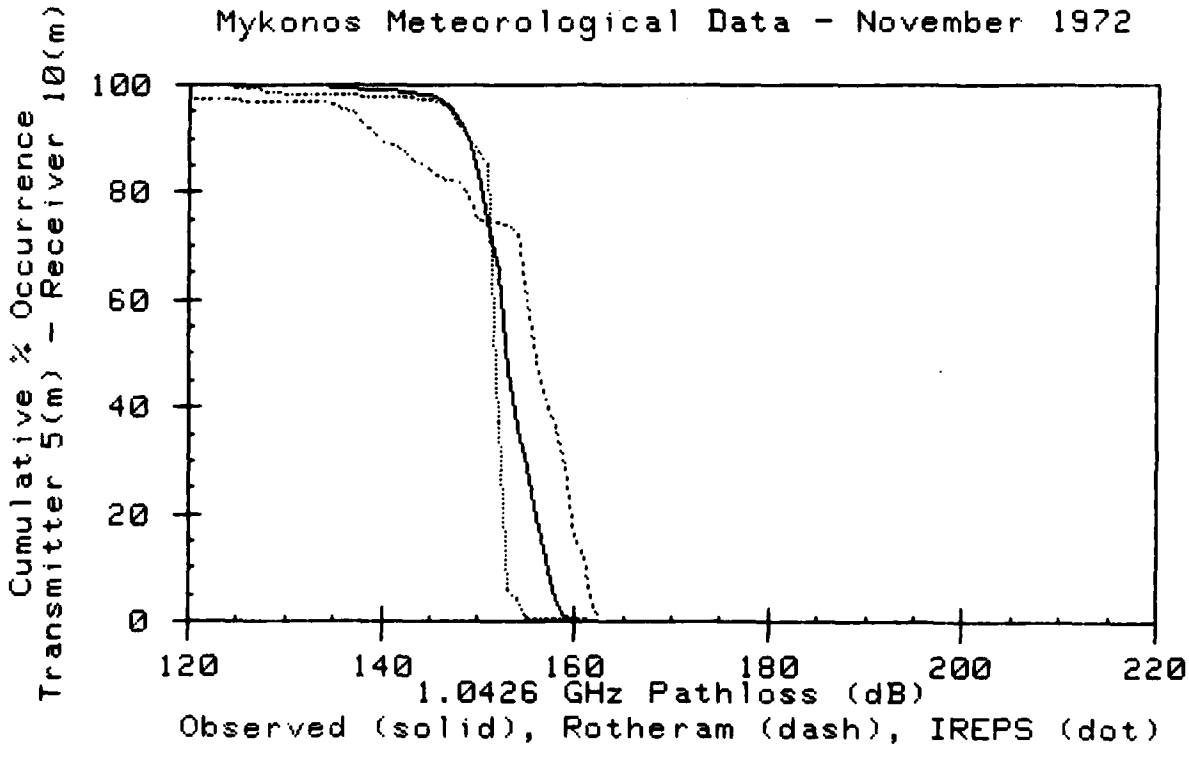

Figure 30. L-band frequency pathloss versus cumulative percent occurrence.

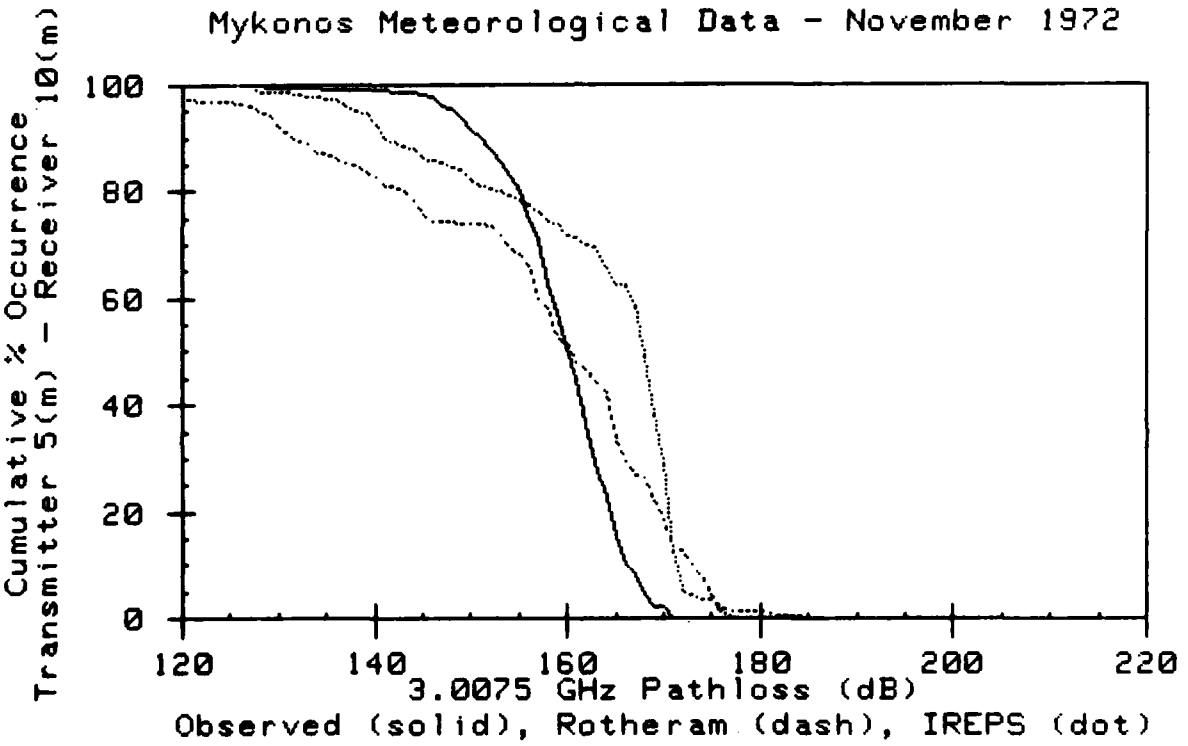

Figure 31. S-band frequency pathloss versus cumulative percent occurrence.

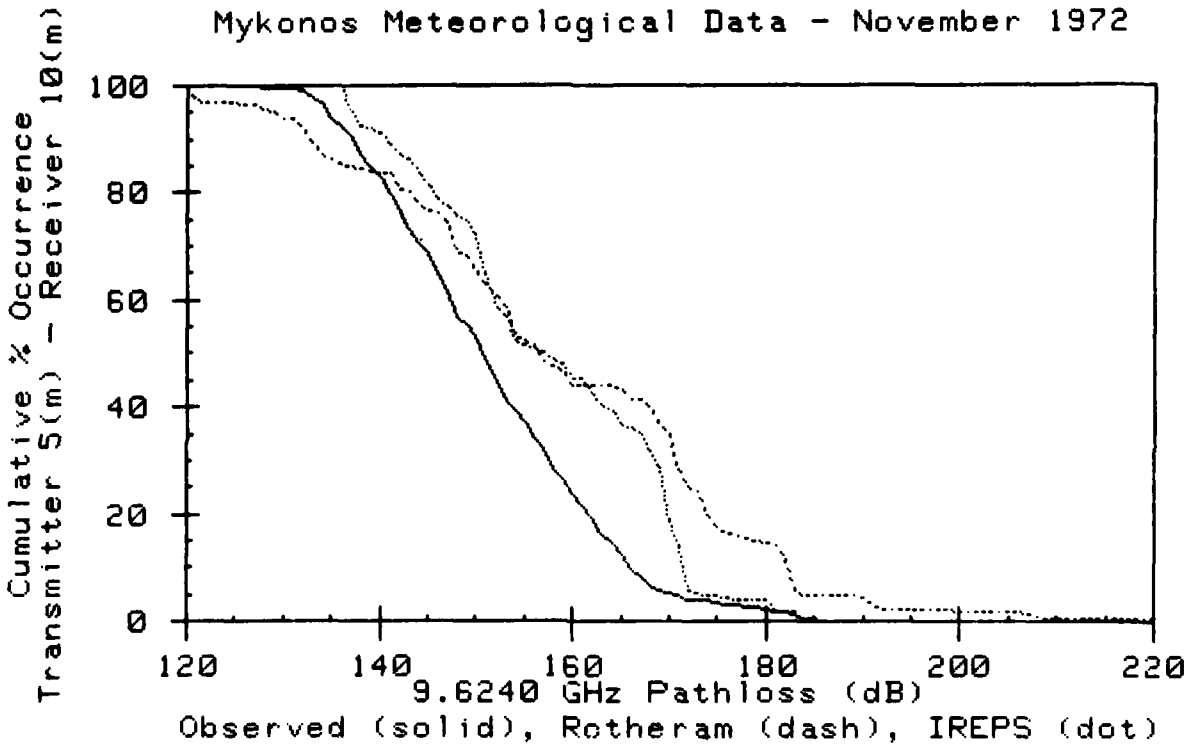

Figure 32. X-band frequency pathloss versus cumulative percent occurrence.

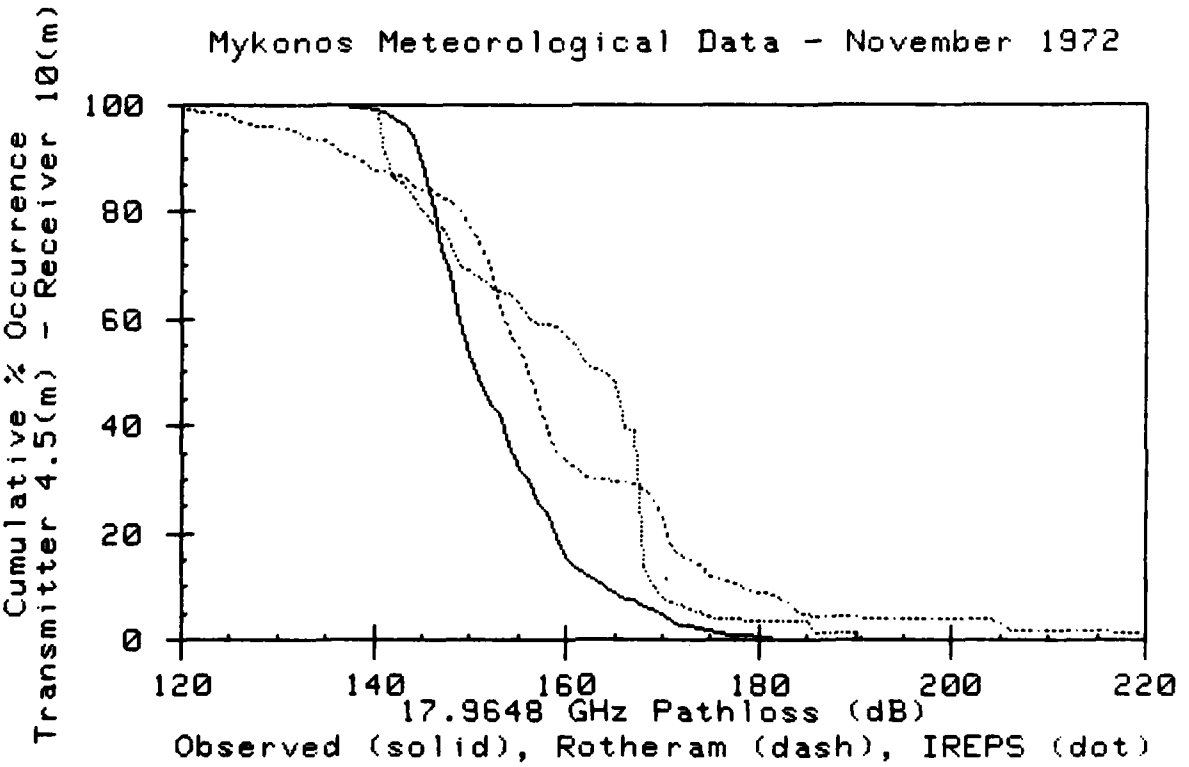

Figure 33. KU-band frequency pathloss versus cumulative percent occurrence.

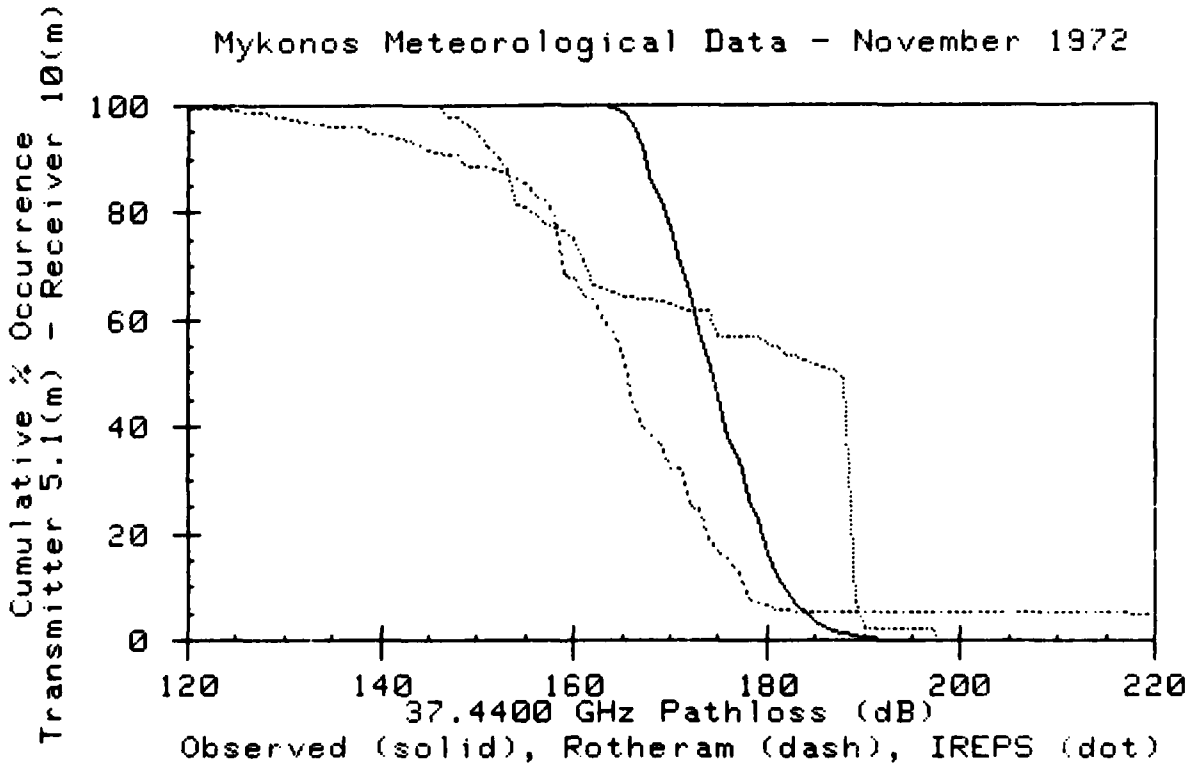

Figure 34. KA-band frequency pathloss versus cumulative percent occurrence.

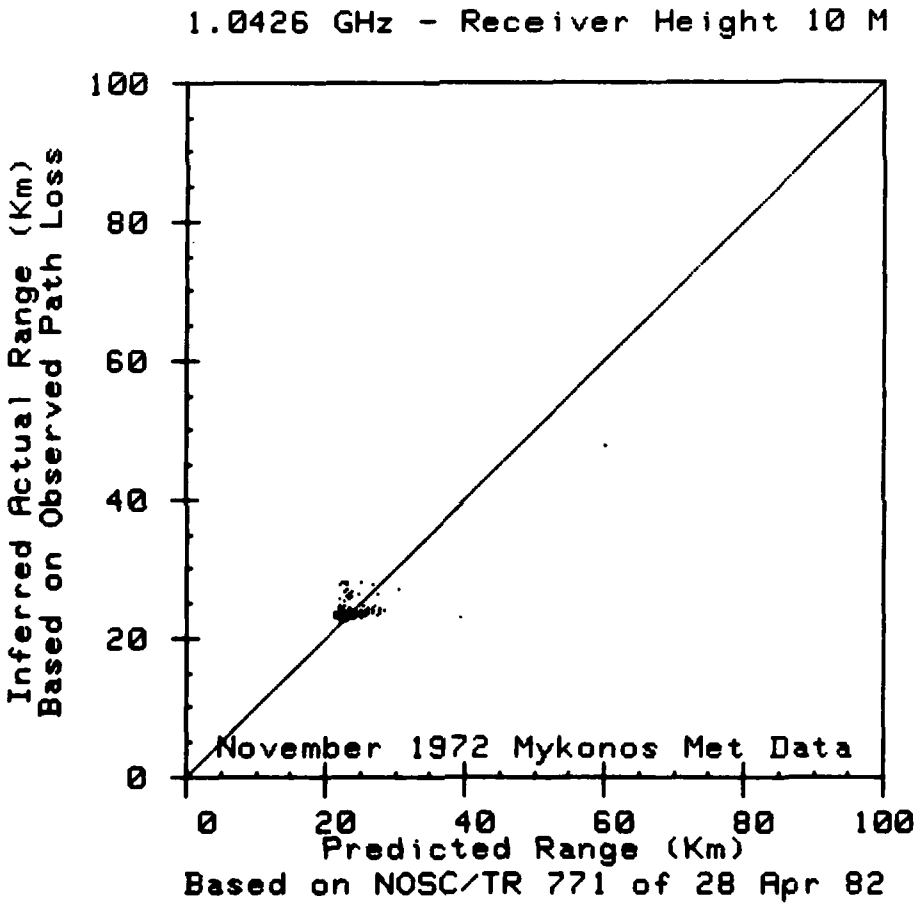

Figure 35. IREPS predicted range versus inferred actual range for L-band frequency.

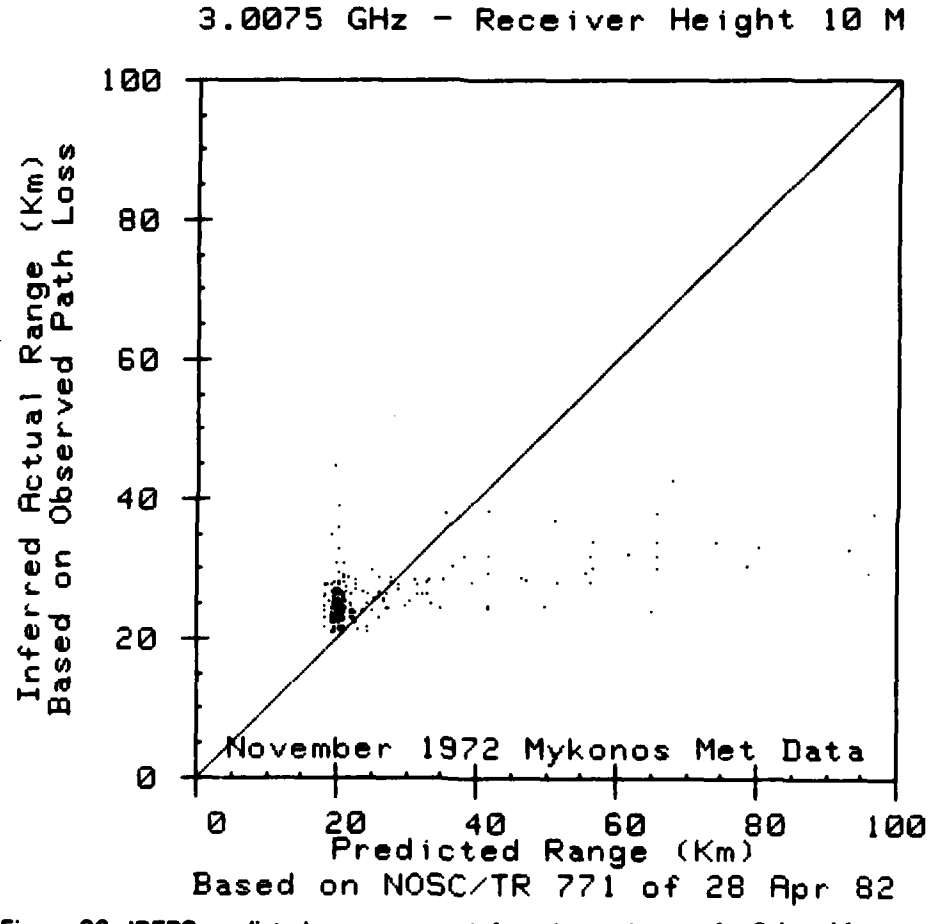

Figure 36. IREPS predicted range versus inferred actual range for S-band frequency.

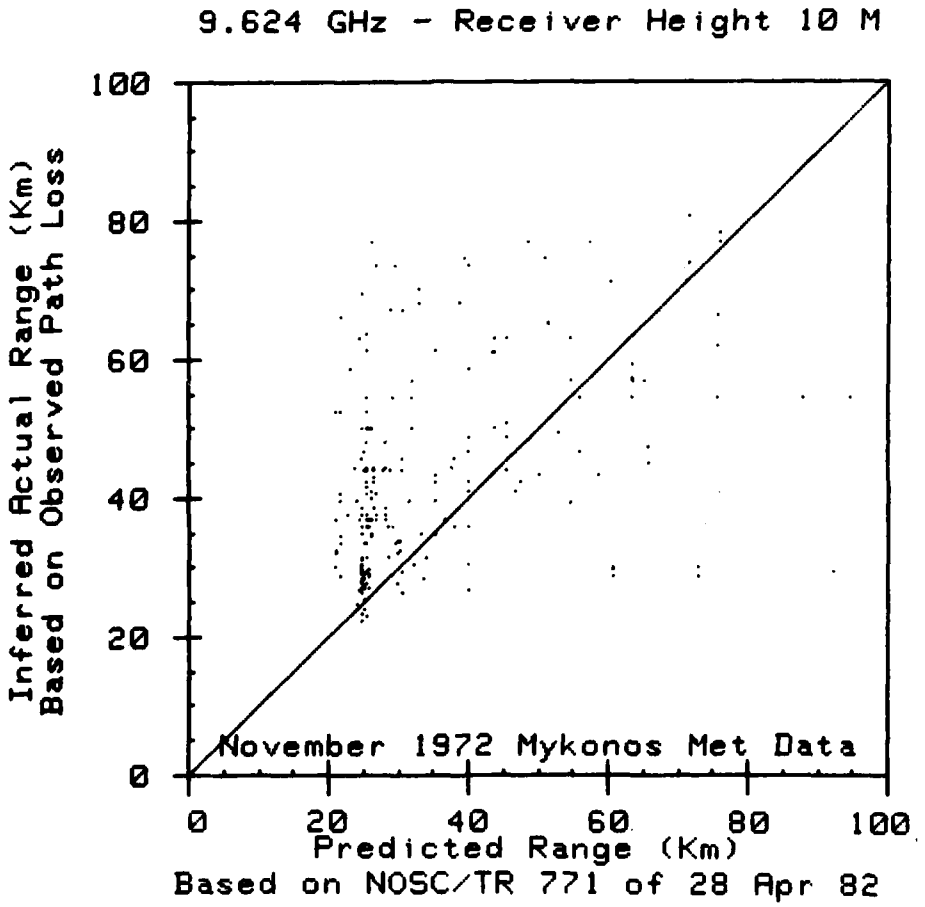

Figure 37. IREPS predicted range versus inferred actual range for X-band frequency.

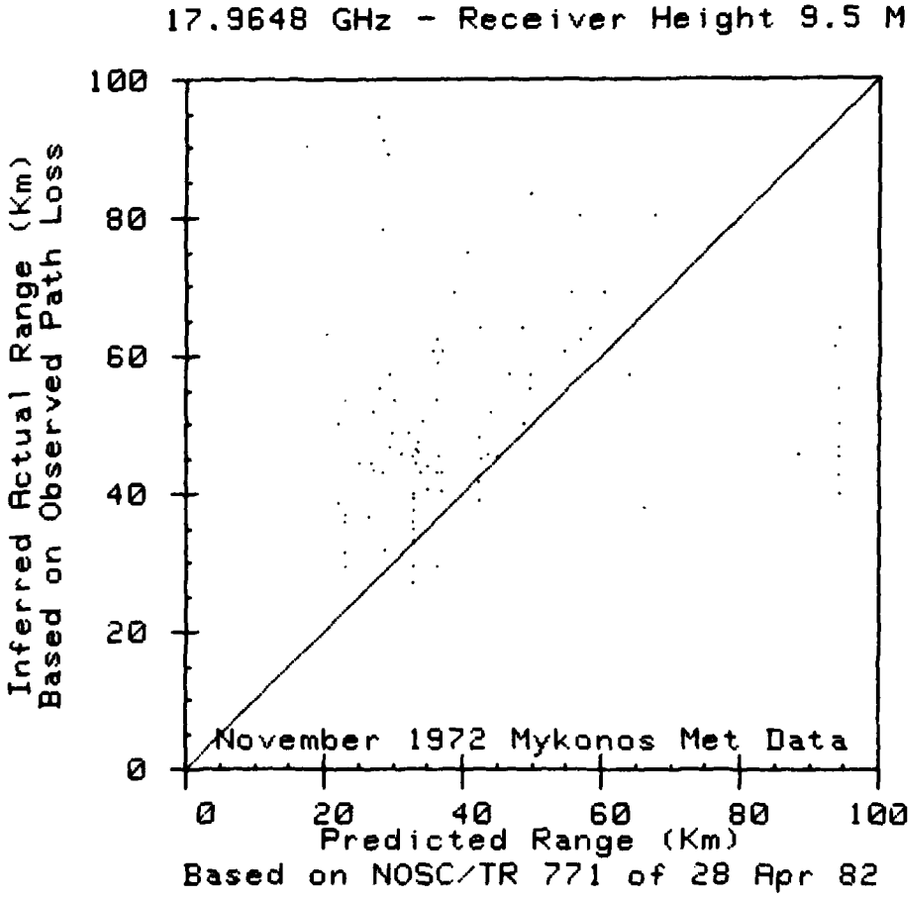

Figure 38. IREPS predicted range versus inferred actual range for KU-band frequency.

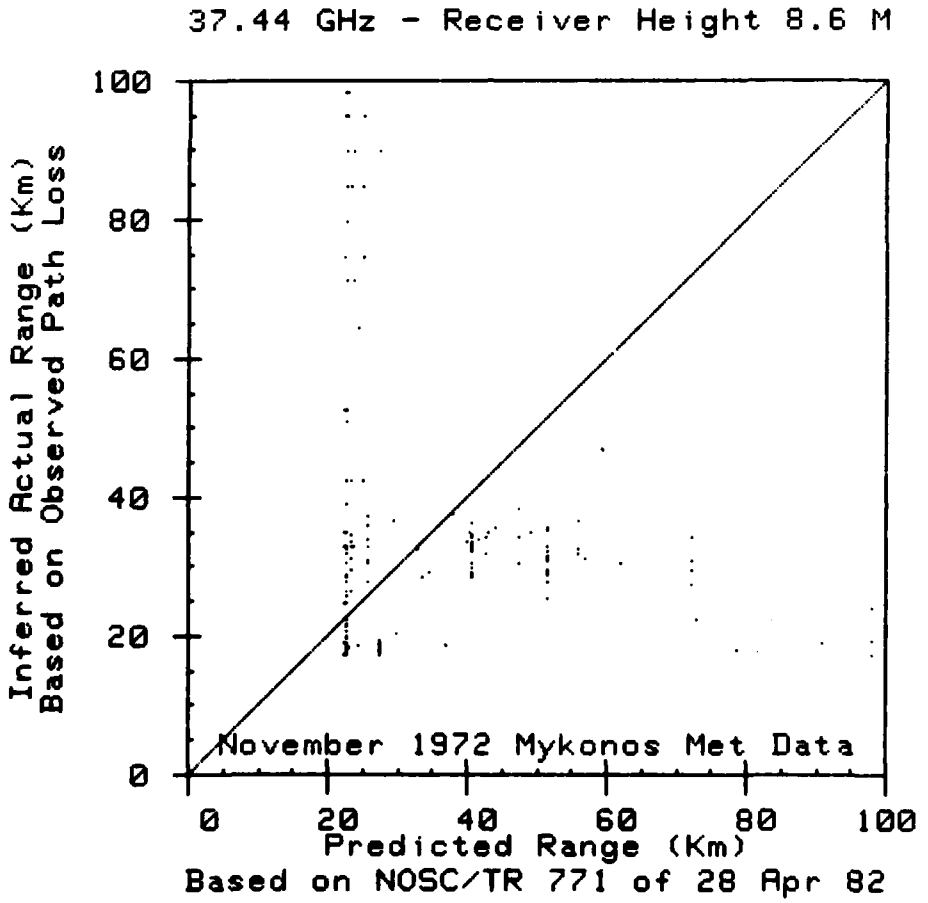

Figure 39. IREPS predicted range versus inferred actual range for KA-band frequency.

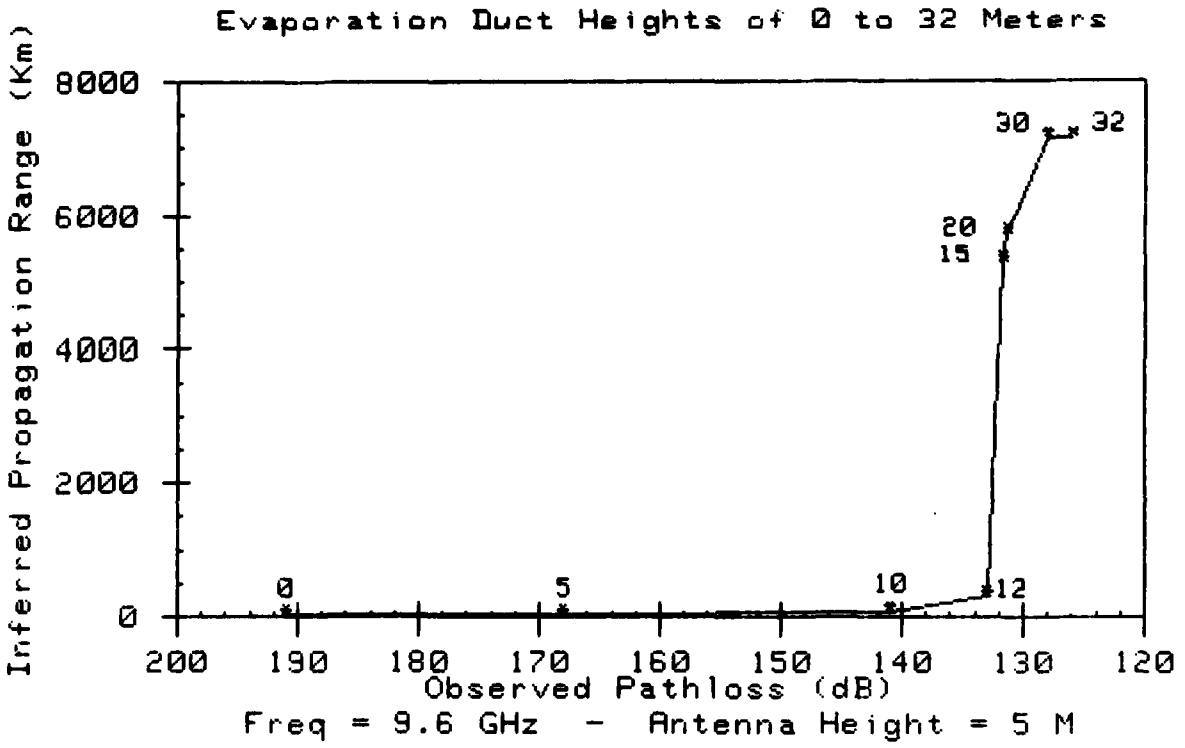

Figure 40. Observed X-band frequency pathloss versus inferred propagation range.

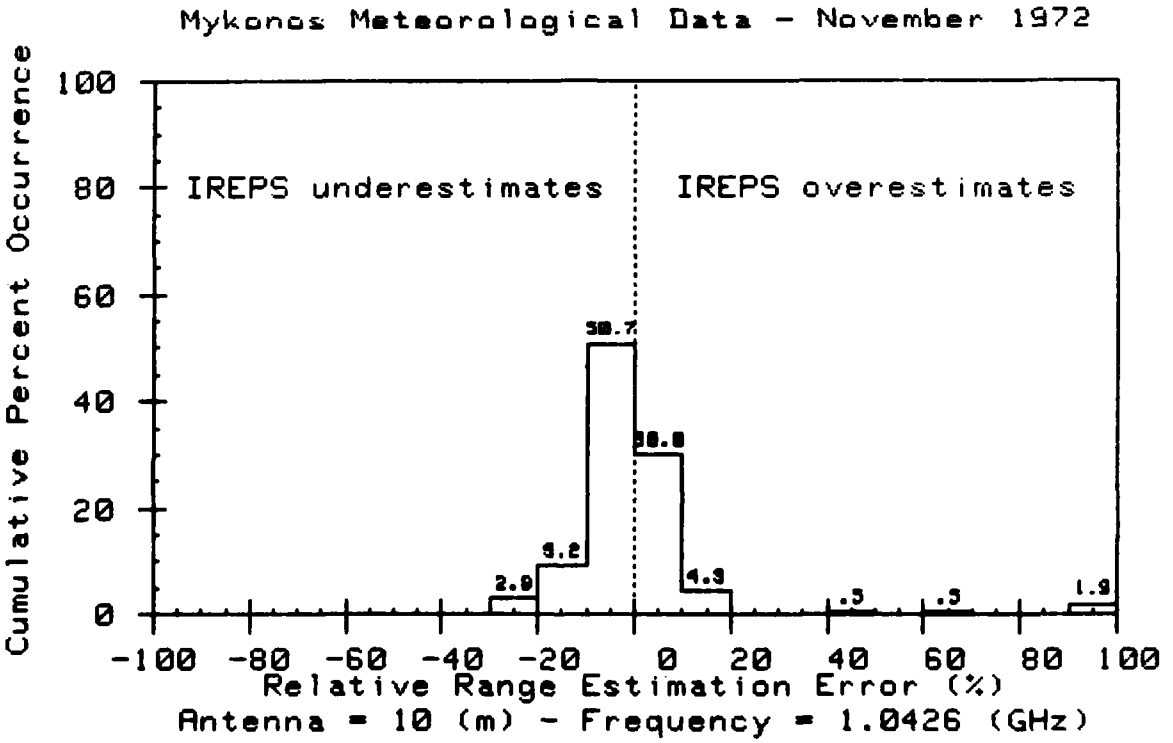

Figure 41. KU-band frequency IREPS relative range error.

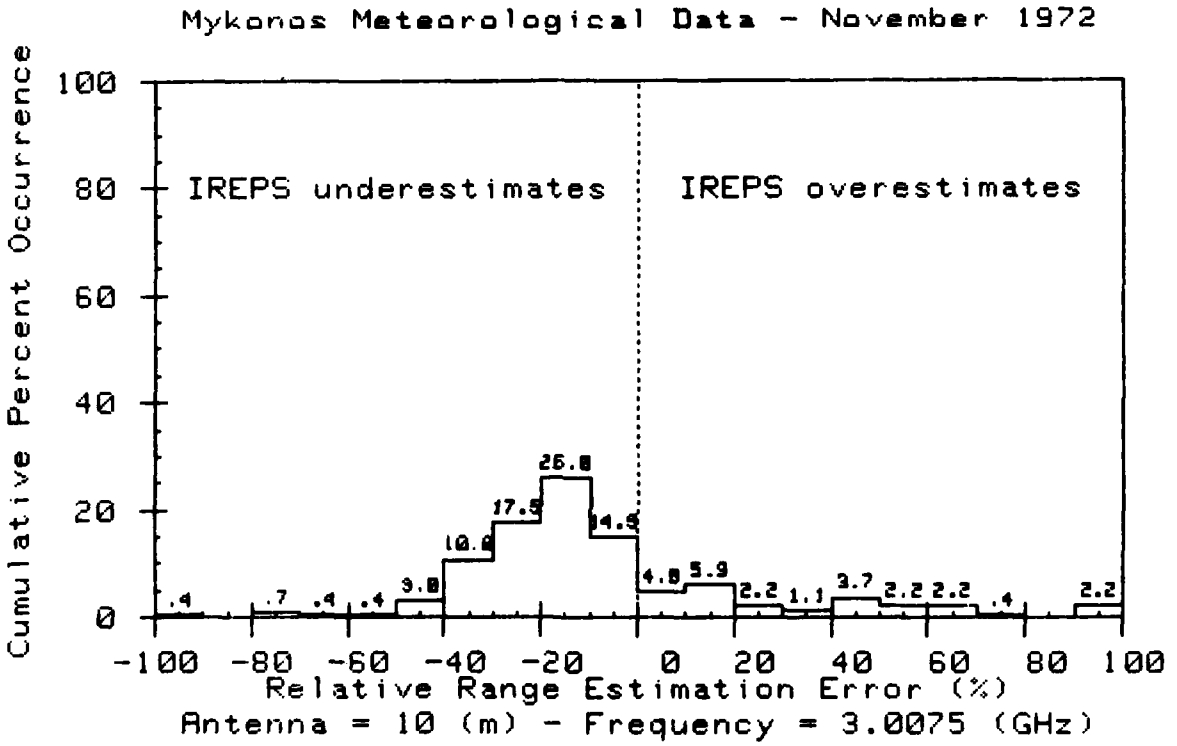

Figure 42. KA-band frequency IREPS relative range error.

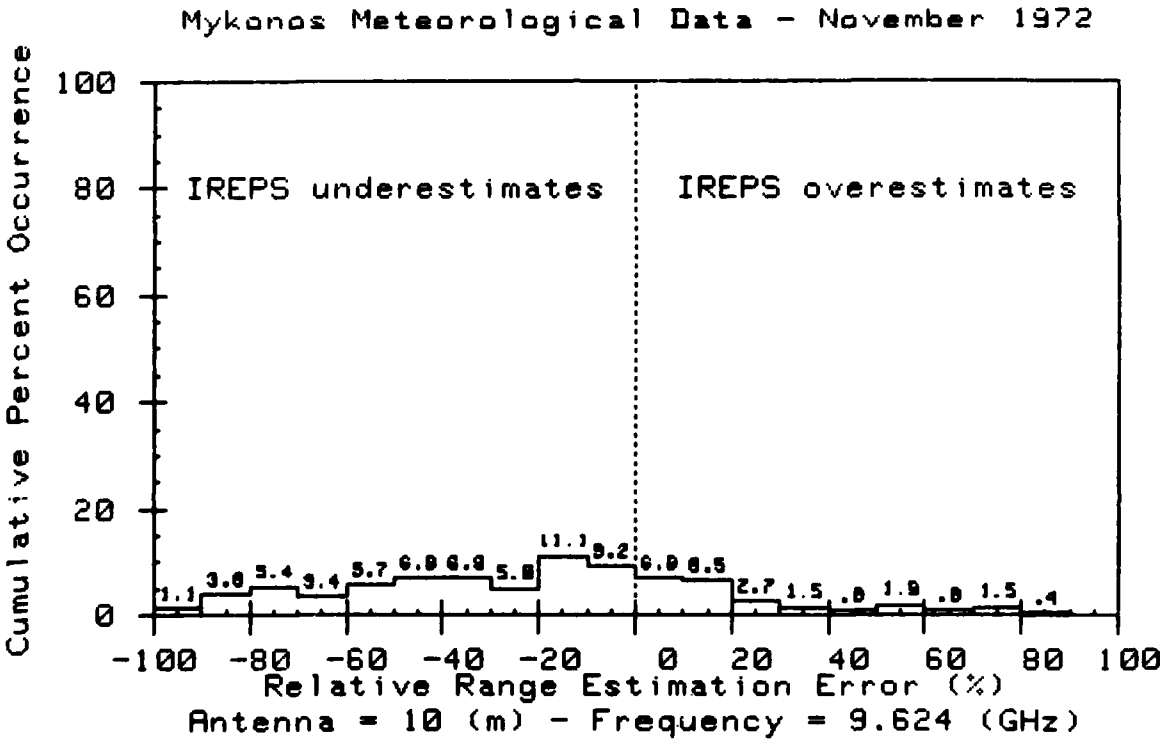

Figure 43. L-band frequency IREPS relative range error.

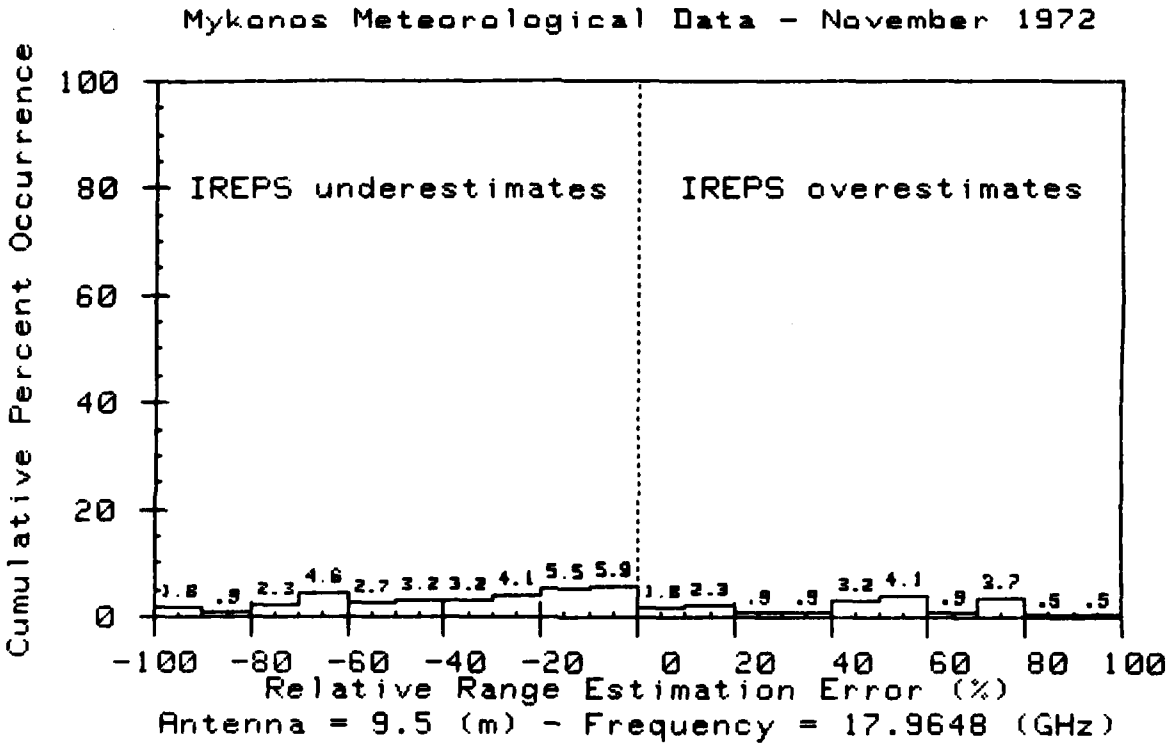

Figure 44. S-band frequency IREPS relative range error.

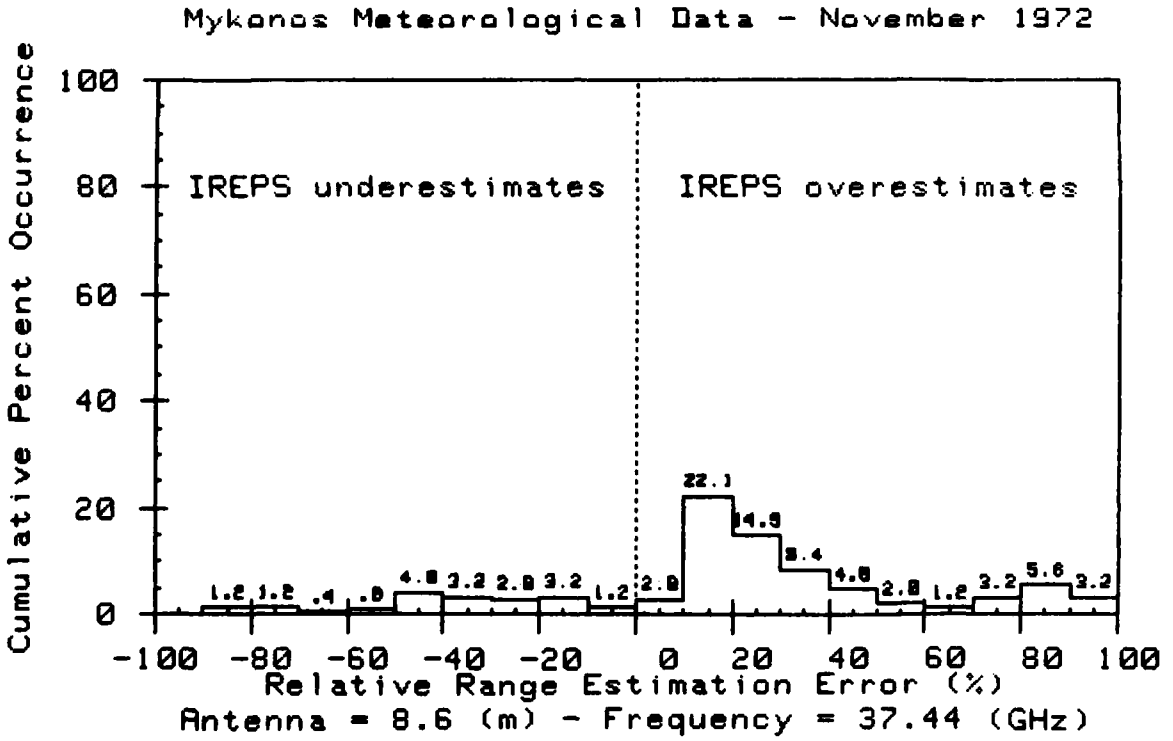

Figure 45. X-band frequency IREPS relative range error.

INITIAL DISTRIBUTION

NAVAL RESEARCH LABORATORY
WASHINGTON, DC 20375
CODE 5330
CODE 5700
CODE 5754

NAVAL AIR SYSTEMS COMMAND
WASHINGTON, DC 20361
AIR-3700

NAVAL SEA SYSTEMS COMMAND
WASHINGTON, DC 20362
SEA-62R13

NAVAL OCEANOGRAPHIC OFFICE
NSTL, MS 39522
CODE 9200

NAVAL WEAPONS CENTER
CHINA LAKE, CA 93555
CODE 3918

NAVAL POSTGRADUATE SCHOOL
MONTEREY, CA 93943
CODE 63DS

NAVAL ENVIRONMENTAL PREDICTION
RESEARCH FACILITY
MONTEREY, CA 93943

PACIFIC MISSILE TEST CENTER
POINT MUGU, CA 93042
CODE 3253

DEFENSE TECHNICAL INFORMATION CENTER
ALEXANDRIA, VA 22314

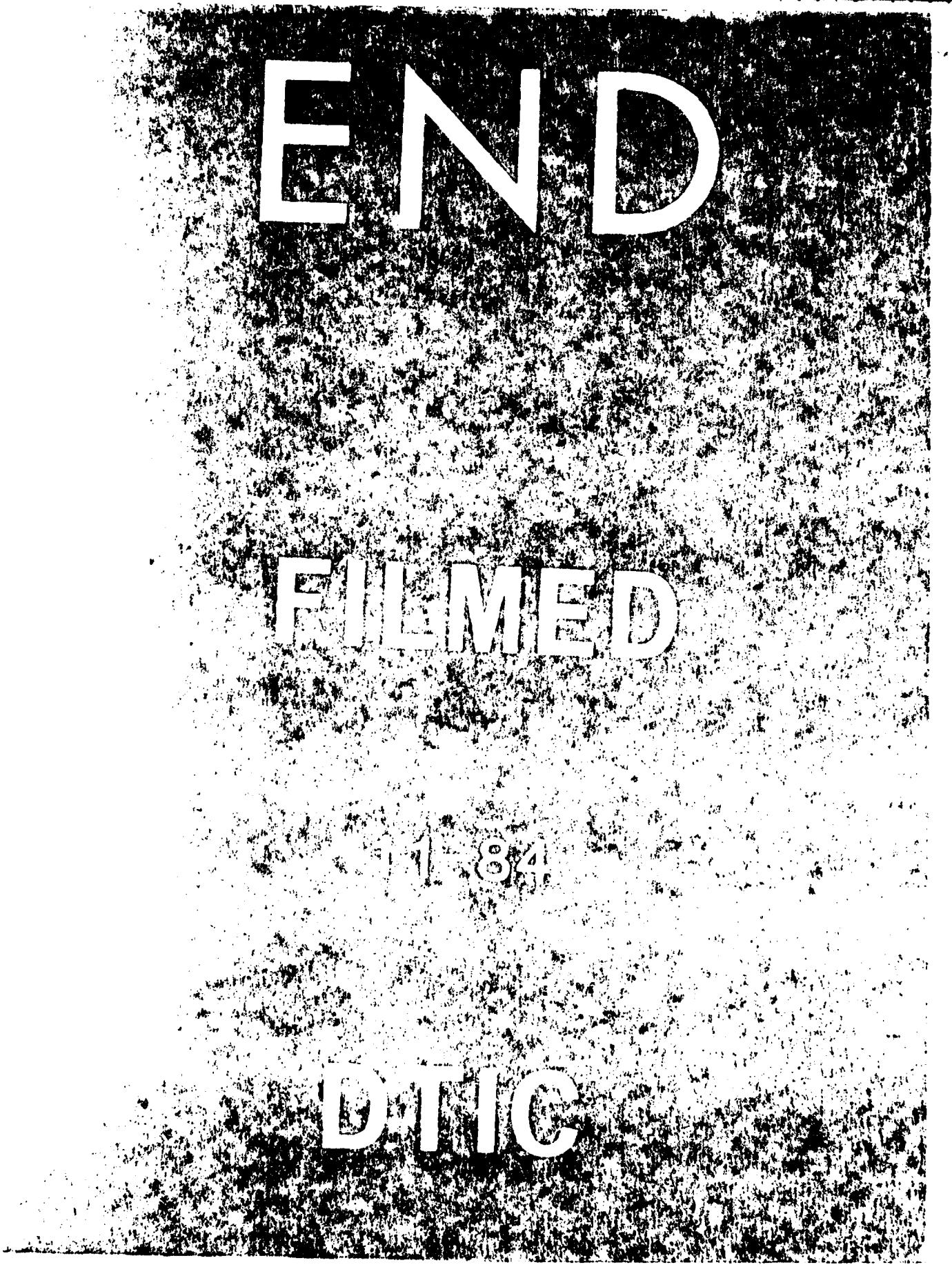
END
FILMED
1-84
DTIC